University of South Bohemia
Faculty of Science

Master thesis

Energy transfer pathways in the intrinsic light harvesting complex of *Amphidinium carterae*

Václav Šlouf

Supervisor: Prof. RNDr. Tomáš Polívka, Ph.D.

České Budějovice 2009

Šlouf, V., 2009: Energy transfer pathways in the intrinsic light harvesting complex of *Amphidinium carterae*. Mgr. Thesis, in English. – 45 p., Faculty of Science, The University of South Bohemia, České Budějovice, Czech Republic.

Annotation:

The main objective of this thesis is to study energy transfer pathways in the intrinsic light harvesting complex of *Amphidinium carterae*. For this purpose, pump-probe spectroscopy was employed using eleven different excitation wavelengths. The thesis includes theoretical background regarding the properties and functions of carotenoids with emphasis on their role in marine photosynthesis. Thereafter, the methods are introduced, femtosecond time-resolved spectroscopy being described in more detail. Finally, transient excitation spectra and other results are presented and discussed.

Prohlašuji, že svoji diplomovou práci jsem vypracoval samostatně pouze s použitím pramenů a literatury uvedené v seznamu citované literatury.

Prohlašuji, že v souladu s § 47b zákona č.111/1998 SB. v platném znění souhlasím se zveřejněním své diplomové práce, a to v nezkrácené podobě elektronickou cestou ve veřejně přístupné části databáze STAG provozované Jihočeskou univerzitou v Českých Budějovicích a na jejích internetových stránkách.

29. dubna 2009

Podpis:

Acknowledgement

I would like to thank my supervisor for leading, patient answering my frequent questions, consulting the results, correcting this thesis, and not least for his friendly approach. All members of the Laboratory of the Femtosecond Spectroscopy in the Institute of Physical Biology in Nové Hrady, namely P. Hříbek, M. Fuciman, and P. Chábera, are acknowledged for their help with many technical matters concerning the femtosecond laser system. Roger Hiller from Macquarie University in Australia is gratefully acknowledged for providing us the samples. Last but not least, thanks belong also to my family and girlfriend.

CONTENTS

LIST OF ABBREVIATIONS AND SYMBOLS

AS	absorption spectrum
c	speed of light in vacuum
C=C	carbon double bond
C_2	rotation about two-fold axis (symmetry element)
CC	carbonyl carotenoid
Chl x (x = a, b, c)	chlorophyll
CT	charge transfer (state)
E	identity (symmetry element)
E	energy
EADS	evolution-associated difference spectra
ESA	excited-state absorption
FCP	fucoxanthin chlorophyll *a*/*c* protein
$\hbar$	reduced Planck constant
i	centre of inversion (symmetry element)
I	intensity (of light radiation)
ICT	intramolecular charge transfer (state)
l	length
LHC	light harvesting complex
N	nuclear wavefunction
n	refractive index
NPQ	non-photochemical quenching
PCP	peridinin chlorophyll *a* protein
PDCP	peridinin diadinoxanthin chlorophyll *a*/*c* protein
Per	peridinin
RC	reaction centre
S	electronic spin wavefunction
S_x (x = 0, 1, N etc.)	molecular state
TA	transient absorption
TAS	transient absorption spectrum
TES	transient excitation spectrum
UC	unidentified carotenoid
v	speed of light in a medium

Δ	increment of quantity
Δt	delay between pump and probe; temporal characterization of the transient absorption signal
λ	wavelength
λ_{trans}	spectral characterization of the transient absorption signal
$\boldsymbol{\mu}$	electric dipole moment operator
$\boldsymbol{\mu}_{nm}$	transition dipole moment
σ_h	horizontal mirror plane (symmetry element)
τ	time delay between two probes
φ	electronic spatial wavefunction
ψ	total molecular wavefunction
ω	angular frequency

1. INTRODUCTION

1.1 The importance of photosynthesis

Photosynthesis is one of the most important processes on the Earth. It is commonly known that green plants utilize photosynthesis to produce organic molecules from inorganic ones. Nevertheless, there are other organisms using this way of gaining organic molecules – algae, many species of Bacteria (including all cyanobacteria), and some species of Archaea. The goal of this study is to provide further insight into the photosynthetic strategies of marine algae[1].

Cell organelles, in which photosynthesis takes place, are called chloroplasts. The light-dependent reactions proceed in the membranes of thylakoids, substructures of chloroplasts. Many protein complexes are embedded in these membranes. Charge separation proceeds in the reaction centres (RCs). To secure that there will be sufficient flux of energy to drive the process of charge separation, there are other pigment-protein complexes surrounding the RCs – the light harvesting complexes (LHCs). While RCs are quite conservative in most of organisms with oxygenic photosynthesis, LHCs exhibit large structural and spectral variability.

Compared to photosynthetic organisms living in the air (higher plants in particular), there are restrictions to underwater photosynthesis. The reason is that water functions as a filter for the red part of the visible spectrum – due to absorption of water molecules. In addition, Stomp et al. (2007) showed that characteristic vibration modes of water molecules further constrain underwater photosynthesis, and consequently have crucially influenced the evolution of phototropic organisms. Nevertheless, in reality also other components in the water column absorb light, mainly gilvin (organic particles) and tripton (inorganic particles). A niche of a particular organism is thus determined by all above-mentioned factors.

Consequently, marine photosynthetic organisms developed different strategies to enhance the efficiency of light harvesting in the blue-green region. The involvement of carotenoids or phycobilins is crucial for this increased utilization of light. This thesis is focused on studying of the involvement of carotenoids in light harvesting and related processes.

[1] Thus from now on only oxygenic photosynthesis will be discussed.

1.2 Light harvesting complexes

A particular LHC[2] is the subject of study presented in this thesis, so some information about antennas will be mentioned in the following paragraphs.

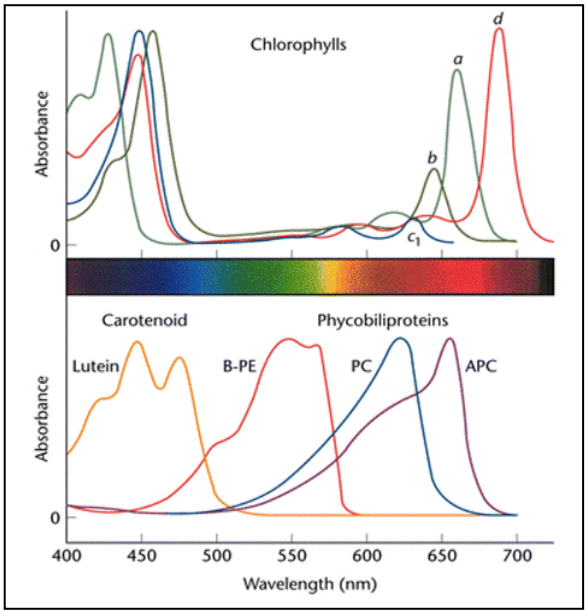

Figure 1: Absorption spectra of the three main classes of pigments.

LHCs are pigment-protein complexes, which were developed by all photosynthetic organisms to trap sunlight because the photon flux density is not high enough to ensure continuous operation of RCs. Three main classes of pigments are contained in LHCs: chlorophylls (Chls), carotenoids, and phycobilins. Their absorption spectra (AS) are shown in Figure 1. Because of the law of conservation of energy, the energy transfer from antennas (and also within them) to the RCs proceeds in the "downhill way" – in particular from the short- to the long-wavelengths absorbing pigments. Additionally, the "redder" the pigment is, the less it is abundant. These two tendencies can be embraced in one term – the "funnel effect" (Fig. 2).

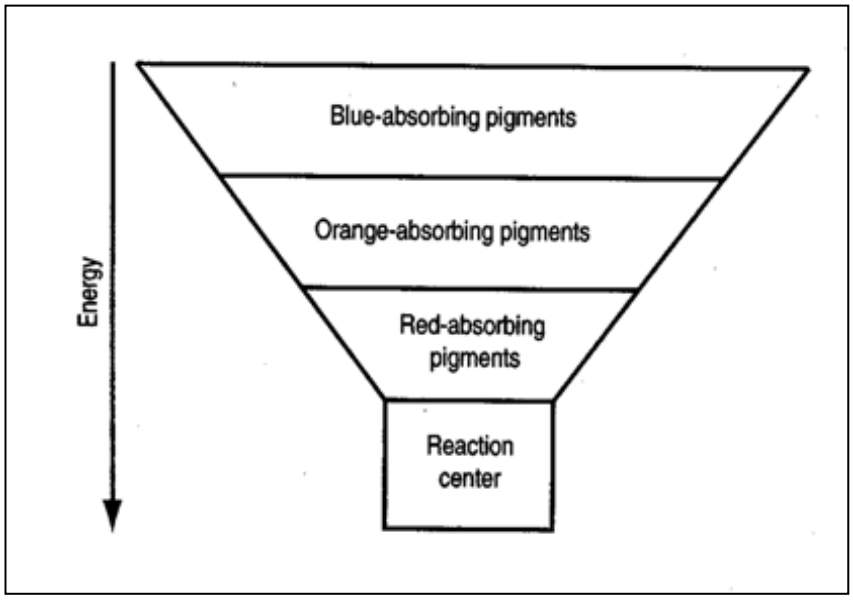

Figure 2: The funnel effect in energy transfer from LHCs to RCs.

What fixes pigments in space is the protein. Apart from its role as scaffolding, it can considerably change the properties of pigments. Most intensively, polarity of the environment and its refractive index correlate with the spectral properties of pigments. Non-covalent bonds of pigments to the protein also influence the spectra. An extreme importance of these phenomena can be demonstrated as follows: while the Q_y band of Chl *a* peaks at 661 nm in diethyl ether (non-polar solvent), the special pair of Chl *a* in the RC of photosystem I has the maximum of ab-

[2] Another name for LHC is an "antenna".

sorbance at around 700 nm. Specific environment-induced effects exist also for carotenoids (section 1.3).

General classification of antennas is as follows (Šetlík et al.):

a) internal
b) peripheral
   ba) intrinsic
   bb) extrinsic.

Internal antennas are quite conservative in organisms with oxygenic photosynthesis. Examples are the pigment proteins CP 43 and CP 47 from photosystem II of higher plants.

Peripheral antennas are very variable among different groups of photosynthetic organisms. The most abundant group of intrinsic antennas can be called LHC superfamily (Green et al. 2003). They are present in Chlorophytes and higher plants where they contain Chl *a* and Chl *b*; in Rhodophytes they encompass only Chl *a*; in Heterokonts, Haptophytes, Cryptophytes, and Dinoflagellates Chl *a* and Chl *c* are incorporated. No less important, carotenoids are bound in these complexes and their content also differs among the above-listed groups. Compared to green plants, algae[3] have much more variable interspecies carotenoid content. Furthermore, the role of carotenoids is not the same in all cases as will be demonstrated in the following examples. In LHCII of higher plants, it is believed that carotenoids have mainly the photoprotective role while in many species of algae they are also of vital importance for light harvesting.

Peripheral extrinsic antennas are represented by two distinct pigment-protein complexes: phycobilisomes and the peridinin Chl *a* protein (PCP). Phycobilisomes appear in Cryptophytes, Rhodophytes, and in almost all cyanobacteria. Particular phycobilins differ in AS, but in concert they cover the whole visible spectrum, thus enabling the well-evolved funnel effect. Last but not least will be described the thoroughly studied PCP. This LHC is contained in Dinoflagellates. PCP contains two pigments – peridinin and Chl *a* – in a stoichiometric ratio 4:1. Consequently, peridinin is the main light harvesting pigment in PCP.

1.3 Carotenoids

The variability of structures and functions of carotenoids is tremendous. Nevertheless, there are certain features characteristic of all of them. The only two elements occurring in all carotenoids are carbon and hydrogen. Another common feature is a linear backbone consisting of carbon atoms alternatively bound by single and double bonds (conjugated π-electron system). Oxygen atoms are

[3] Except for green algae – higher plants are their ancestors, so the pigment content of both these groups is the same.

present in some of them – such compounds are called xanthophylls. Xanthophylls are contained in the LHC, on which the study presented in this thesis was focused (Figs. 3C, 3D).

A lot of effort has been put to disentangle the manifold of excited states of carotenoids because of the close connection with their functions. Thus more attention will be dedicated to this topic in the next paragraphs. Thereafter, a special group of carotenoids (carbonyl carotenoids) often employed by marine photosynthetic organisms will be described. Finally, main functions of carotenoids connected with photosynthesis will be explained.

1.3.1 Typical features of excited states of carotenoids[4]

After absorbing a photon, a carotenoid is excited into the second excited state, denoted S_2. The S_0-S_2 transition, where S_0 is the symbol for the ground state, is strongly allowed, and is responsible for absorption in the blue-green region, which is typical for carotenoids. As a consequence, organisms possessing huge amount of carotenoids typically have colours from yellow or red.

C_{2h}	E	C_2	i	σ_h	Rotations, translations
A_g	1	1	1	1	R_z
B_g	1	-1	1	-1	R_x, R_y
A_u	1	1	-1	-1	T_z
B_u	1	-1	-1	1	T_x, T_y

Table 1: Character table of the C_{2h} point symmetry group.

What is behind the allowedness of this transition? To find out, some information from the group theory has to be dropped. Carotenoids belong to the C_{2h} idealized point symmetry group, which contains the following symmetry elements: identity (E), a two-fold symmetry axis (C_2), a centre of inversion (i), and a horizontal mirror plane (σ_h). The characters (i.e. 1 or -1) of symmetry operations of the irreducible representation are summarized in the so called character table (Table 1). Each combination of characters forming a row in the character table is given a symbol. Thus, the *A*s and *B*s are used to distinguish the sign of the character of rotation around the two-fold axis. Similarly, the subscripts *g* and *u* are used to distinguish the characters of inversion. Now, which species are given the particular symbols? For our purposes, these will be orbitals, states, and components of transition dipole moment vectors. From knowledge of shapes of orbitals it is possible to determine whether a symmetry operation causes the exchange of positive and negative parts of orbitals (this is the antisymmetric case, which is given the character -1) or whether their position remains unchanged (symmetric case, character 1). The orbital

[4] Carbonyl carotenoids comprise a very special group and many characteristics discussed in section 1.3.1 are not valid for them. As a consequence, a special section 1.3.2 is dedicated to them.

is then given a symbol, e.g. A_g, corresponding to specific combination of characters. Consequently, from knowledge of orbitals taking part in an electronic transition, we can easily deduce the symmetry of the particular excited state, which is the product (standing for multiplying of involved characters) of symmetries of orbitals involved in the transition[5].

We are getting at the solution of the problem whether a transition is allowed or not. The crucial quantity determining the allowedness of a transition is the transition dipole moment, $\boldsymbol{\mu}_{nm}$; $\boldsymbol{\mu}_{nm} = \langle\psi_n|\boldsymbol{\mu}|\psi_m\rangle$, where ψ_m and ψ_n are wavefunctions of the initial and final states, respectively, and $\boldsymbol{\mu}$ is the electric dipole moment operator). Under Born-Oppenheimer approximation, it is possible to factorize the total wavefunction: $\psi = \varphi SN$, the multiplicands standing for electronic spatial, electronic spin, and nuclear wavefunctions, respectively. The transition dipole moment thus becomes the following form: $\boldsymbol{\mu}_{nm} = \langle\varphi_n|\boldsymbol{\mu}|\varphi_m\rangle\langle S_n|S_m\rangle\langle N_n|N_m\rangle$. Because the electric dipole moment operator $\boldsymbol{\mu}$ affects only the electronic spatial wavefunction, the final integral in focus will be $\langle\varphi_n|\boldsymbol{\mu}|\varphi_m\rangle$, φ_m and φ_n standing for initial and final electronic spatial wavefunctions, respectively. The symmetries of states are possible to be found out according to the above mentioned method, and for excited states of carotenoids holds the following: S_0 state is of A_g (denoted $1A_g$ because it is the first state) and S_2 of B_u ($1B_u$) symmetry. The components of the dipole moment vector transform like transitions (Table 1). The crucial condition for the function of the kind $\varphi_n\mu_x\varphi_m$ to yield a nonzero result is that it must transform as a totally symmetric member of the C_{2h} point group, i.e. as A_g.

Let us look at the S_0-S_2 (A_g-B_u) transition. The overall symmetry of the function $\varphi_n\mu_x\varphi_m$ will be $B_uB_uA_g=A_g$. Thus the above-mentioned condition is fulfilled, so the transition is symmetry-allowed. The same result is received for the function $\varphi_n\mu_y\varphi_m$ ($B_uB_uA_g=A_g$), but not for $\varphi_n\mu_z\varphi_m$ ($B_uA_uA_g=B_g$), which turned out to be symmetry forbidden. Nevertheless, only one of the three expressions being non-zero is enough for the transition to be overall symmetry allowed[6] (Gilbert and Baggott 1991). It should be mentioned, however, that the transition may turn out to be forbidden for different reasons. In particular, two other contributors to the transition dipole moment were omitted (overlap integrals related to the electron spin and nuclear wavefunctions). Zero value of any of them also leads to the fact that a transition is forbidden.

In contrast, the lowest-lying electronic excited state, S_1, is of A_g symmetry, so it possesses the same symmetry as the ground state. With methods introduced in the foregoing paragraphs it is possible to prove that S_0-S_1 transition is symmetry-forbidden. The strictness of the assertion that some

[5] An example will illustrate the situation. Let us assume that orbitals of A_g and B_g symmetry are involved in forming an excited state (one electron in the former and second in the latter orbital). By multiplying of characters in the first row by corresponding characters in the second row (from Table 1) originates again a quaternion (1; -1; 1; -1), possessing the B_g symmetry, which is the symmetry of the excited state.

[6] The transition is, however, polarized because it is not allowed along all three axes.

states are not allowed follows from the fact that it is only an approximation. In reality, carotenoids are not absolutely symmetric in terms of the idealized C_{2h} point symmetry group. Deviations from the full symmetry result for example in weak allowedness of S_1-S_0 transition, which was widely used to study S_1 state properties until late 1990s. Nevertheless, although determination of the S_1 state features is possible, it is still difficult. There are four main methods enabling to overcome the problems to some extent so that the information about S_1 state can be obtained: fluorescence spectroscopy (Bondarev and Knyukshto 1994)[7], resonance Raman spectroscopy (Gaier et al. 1991), two-photon absorption (Zimmermann et al. 2002), and femtosecond time-resolved spectroscopy (Polívka et al. 1999).

From the foregoing paragraphs follows that most of carotenoids possess unusual spectroscopic properties compared to the majority of other organic molecules, which can be demonstrated by means of the Kasha-Vavilov rule. This rule says that fluorescence emanates from the lowest-lying electronic excited state of the molecule. Fluorescence from S_1 state of carotenoids is very weak compared to S_2 fluorescence, resulting in avoiding the rule. Strictly speaking, there is the critical conjugation length of eight carbon double bonds above which S_2 emission dominates (Frank et al. 2002).

1.3.1.1 The S_2 state

Properties of the S_2 state, discovered mainly from measurements on carotenoids in solution, will be briefly summarized in this section:

1) Conjugation length:
   - the longer the conjugation length, the lower the energy and (consequently) lifetime
   - resolution of the vibrational structure of AS not significantly influenced
2) Solvent polarizability (tendency of the charge distribution of the molecule to be distorted because of the presence of an external electric field):
   - the higher the polarizability, the lower the energy and lifetime
3) Solvent polarity:
   - S_2 state not significantly affected

[7] Weak carotenoid fluorescence had been known decades ago, but it had not been given in connection with S_1 state.

1.3.1.2 The S_1 state

Properties connected with the S_1 state of carotenoids[8] are summarized below:

1) Conjugation length:
   - the same tendency for energy and lifetime as for S_2
   - decrease of S_1 energy somewhat steeper than for the S_2 state resulting in larger S_1-S_2 energy gap for longer carotenoids
   - carotenoids shorter than eight conjugated C=C bonds: domination of S_1 emission
2) Solvent polarizability and polarity:
   - S_1 state not influenced to a considerable extent

Before another chapter will be introduced, it should be mentioned that diadinoxanthin, a carotenoid present in LHC that is the subject of this thesis, is a xanthophyll with "normal" carotenoid properties, so all above-mentioned characteristics are valid also for diadinoxanthin.

1.3.2 Carbonyl carotenoids

Carbonyl carotenoids (CCs) comprise a very special group of carotenoids. Their uniqueness lies in the fact that they have a carbonyl group *in conjugation*. In particular, the presence of the oxygen atom is crucial because it has the second highest value of electronegativity among elements, so it considerably withdraws electrons from the adjacent atoms. Consequently, spectroscopic and dynamic properties of CCs are very sensitive to the solvent environment, particularly to its polarity.

While in non-polar solvents the properties of CCs are rather unaffected compared to other carotenoids, considerable changes appear in polar solvents. Currently, such behaviour is ascribed to the presence of charge transfer (CT) state(s). Their existence has been confirmed by ab initio calculations using time-dependent density functional theory (Vaswani et al. 2003)[9]. Because the CT states possess significant dipole moment, they are stabilized in the polar environment, which is equivalent to lowering of their energy.

The very typical and most thoroughly studied CC is peridinin (Fig. 3C). Its characteristic features are seven C=C bonds in conjugation, a lactone ring, an allene moiety, and two β-rings. Figure 3C also illustrates a feature of CCs, which is a considerably violated symmetry. Peridinin will be used as an example in the following paragraphs. This carotenoid is also contained in the LHC, which is the subject of this thesis, so properties of CCs will be described below in more detail.

[8] Again most of the properties were found out from measurements on carotenoids in solution.
[9] Nevertheless, only the CT state adjacent to the S_1 state (or even coupled with it as will be remarked below) is described here in more detail because of its importance in energy transfer to Chls.

1.3.2.1 Properties of excited states of carbonyl carotenoids

A typical feature of CCs in polar solvents is the loss of vibrational structure of their AS. In non-polar solvents the shape of the AS with typical three peaks is similar to other carotenoids. However, the partial negative charge on the oxygen is stabilized in polar solvents. Consequently, enhanced repulsion induces the conformational disorder, leading to spectral broadening and loss of the vibrational structure (Frank et al. 2000). In addition, the whole AS of CCs are slightly red-shifted compared to those of their counterparts which lack the carbonyl group. This fact can be in some cases explained by the presence of some conformers involved in hydrogen bonding (Zigmantas et al. 2003).

Nevertheless, the most attention has been paid to the S_1 state of CCs. One of the reasons is that this state plays a crucial role in energy transfer to Chls in LHCs containing peridinin. Features typical to many of CCs are as follows:

1) Most of the CCs studied so far exhibit S_1 emission.
2) The S_1 lifetime of some CCs strongly depends on the solvent polarity. While the S_1 lifetime of peridinin is 160 ps in non-polar solvents (n-hexane or CS_2), an increase of polarity causes substantial shortening of the S_1 lifetime to ~10 ps (methanol or acetonitrile; Bautista et al. 1999). Although a lot of problems remain, many researchers agree that an intramolecular charge transfer (ICT) state is responsible for such behaviour. The ICT state lies below the S_1 state and very close to it. Thus this additional channel causes partial relaxation from S_1 to ICT and, as a consequence, shortening of the S_1 lifetime.

   Further studies revealed that the ICT state is very strongly coupled to the S_1 state. Consequently, especially in LHCs both states behave as one state, usually denoted as S_1/ICT (Zigmantas et al. 2003). The recent model of the arrangement of excited states of peridinin indicates that the ICT part of the S_1/ICT state does not "appear" when the CC is exposed to polar environment (Frank et al. 2000). It is present permanently, but not populated in non-polar solvents.

   The finding mentioned above is of crucial importance for photosynthetic organisms employing CCs. It might enable them to optimally tune the protein environment of the CC in such a way that the energy transfer efficiency to other pigments (Chls) is very high (Polívka et. al 2006).

Finally, it should be emphasized that only two features are common to all so far studied CCs: asymmetric broadening and loss of the vibrational structure of their AS. On the other hand, variation of the S_1 lifetime depends on the structure of a particular CC – e.g. spheroidenone does not exhibit

any changes in S_1 lifetime when measured in polar and non-polar solvents (Polívka and Sundström 2004).

1.3.3 Light harvesting function of carotenoids

Light harvesting ability of carotenoids is vitally important for some underwater photosynthetic organisms (e.g. for Dinoflagellates), for which following requirements are necessary to be met: 1) maximum of absorption in the blue-green[10] region (restrictions to underwater photosynthesis are described in section 1.1), which is reached by excitation of a carotenoid into its S_2 state; 2) a lower state has to be high enough to be able to transfer energy to Chl *a*; 3) the state functioning as the energy donor must not relax too fast[11] to accomplish efficient energy transfer.

It is not surprising that CCs are very often employed by marine organisms. In algae, the most abundant CCs are fucoxanthin, siphonaxanthin, and peridinin. As mentioned above, features of their excited states are determined by properties of the environment, mainly by polarity. In particular, surrounding polar amino acids and involvement of hydrogen bonding induce the stabilization (i.e. shift to lower energies) of the ICT part of the S_1/ICT state (Zigmantas et al. 2001), considered as a key factor ensuring high efficiency of CC-Chl energy transfer. The protein properties also cause the red shift of the S_0-S_2 transition, maximizing the absorption in the spectral region of interest. Hence, the red-shifted S_2 state (the first condition is met) relaxes fast into the S_1/ICT state because of narrow S_2-S_1/ICT energy gap[12]. The S_1/ICT state, being high enough to ensure energy transfer to Chl, decays on the picosecond time scale (Bautista et al. 1999), which is long enough[13] for an energy transfer mechanism to be a successful competitor (thus the other two conditions are met). To summarize, the protein environment can "tune" the properties of a CC in such a way that the above-mentioned conditions are fulfilled, resulting often in very high efficiency of CC-Chl energy transfer (e.g. in PCP).

1.3.4 Photoprotective function of carotenoids

The photosynthetically important excited state of a Chl molecule is a singlet state. The lifetime of this state is ~10^{-9} s. Nevertheless, there is a probability that a triplet state will be generated via the intersystem crossing. The triplet lifetime is substantially longer (on the order of 10^{-3} s), which offers a possibility of diffusion-limited interaction with molecular oxygen possessing the triplet ground-state organization. Oxygen in its ground state does not react with most of other molecules at room

[10] In particular, the redder part of the blue-green region is more desiring because it is inaccessible by Chls.
[11] Not that fast as, for instance, relaxes the S_2 state.
[12] With increasing proximity of states rises the internal conversion rate (energy gap law).
[13] But, compared to similarly long carotenoids, this is a short lifetime.

temperature because of the law of conservation of spin quantum number. Nevertheless, triplet Chl can pass the excitation on triplet oxygen, forming singlet excited state of molecular oxygen and singlet ground state of Chl. Singlet oxygen is very reactive and harmful to living matter. Carotenoids are able to quench both triplet Chl and singlet oxygen (Cogdell 1985), thereby preventing oxidative damage of photosynthetic systems.

The other intensively discussed photoprotective role of carotenoids is in non-photochemical quenching (NPQ), i.e. quenching of singlet Chl excitations, best known from LHCII of higher plants. Under high light conditions, violaxanthin is converted into zeaxanthin in the so-called xanthophyll cycle. Although the fundamental mechanism is not yet satisfactorily understood, it is clear that zeaxanthin mediates the quenching of Chl *a* excited state because when present, Chl *a* fluorescence lifetime decreases (Bassi and Caffari 2000). Another xanthophyll cycle operates in many species of algae, where diatoxanthin is formed at the expense of diadinoxanthin (Arsalane et al. 1994).

1.4 Light harvesting complexes of Dinoflagellates

Herein, having all important information collected, it is possible to introduce the subject of interest of this thesis – the peridinin diadinoxanthin chlorophyll *a*/*c* protein (PDCP[14]). It is the peripheral intrinsic LHC (see section 1.2) of many species of the division Dinoflagellates (alternatively called Dinophyta). This study is focused on PDCP of *Amphidinium carterae*, which is a member of the class Dinophyceae.

Nonetheless, apart from PDCP, most photosynthetic Dinoflagellates comprise also the other kind of LHC – the PCP. A lot of research has been carried out on PCP for many reasons. It is structurally unique when compared with other LHCs, mainly because of its unusually high carotenoid content. Its structure has been resolved to 2.0 Å (Hofmann et al. 1996), which revealed a trimeric organization of PCP, and enabled the deeper study of energy transfer. The efficiency of peridinin-Chl *a* energy transfer is very high, reaching almost 100% (Koka and Song 1977). Such a high efficiency is mainly ascribed to unique properties of peridinin known for polarity-dependent spectroscopic characteristics (see section 1.3.2). Thus optimal tuning of spectroscopic properties by the interaction with protein can be reached, resulting in both effective absorption in the blue-green region and efficient peridinin-Chl *a* energy transfer.

[14] This abbreviation is used as an analogy to PCP and FCP (see below). Although the membership to the LHC superfamily is not apparent from the abbreviation, it matches the pigment composition.

Compared to PCP, PDCP has been studied much less. The crystal structure is not known. The pigment composition of PDCP according to Hiller et al. (1993) is shown in Table 2. The structures of the components are shown in Figure 3.

Pigment	Chl *a*	Chl *c*[15]	Peridinin	Diadinoxanthin
Number of molecules per protein	7	4	12 (10)	2

Table 2: Pigment composition of PDCP.

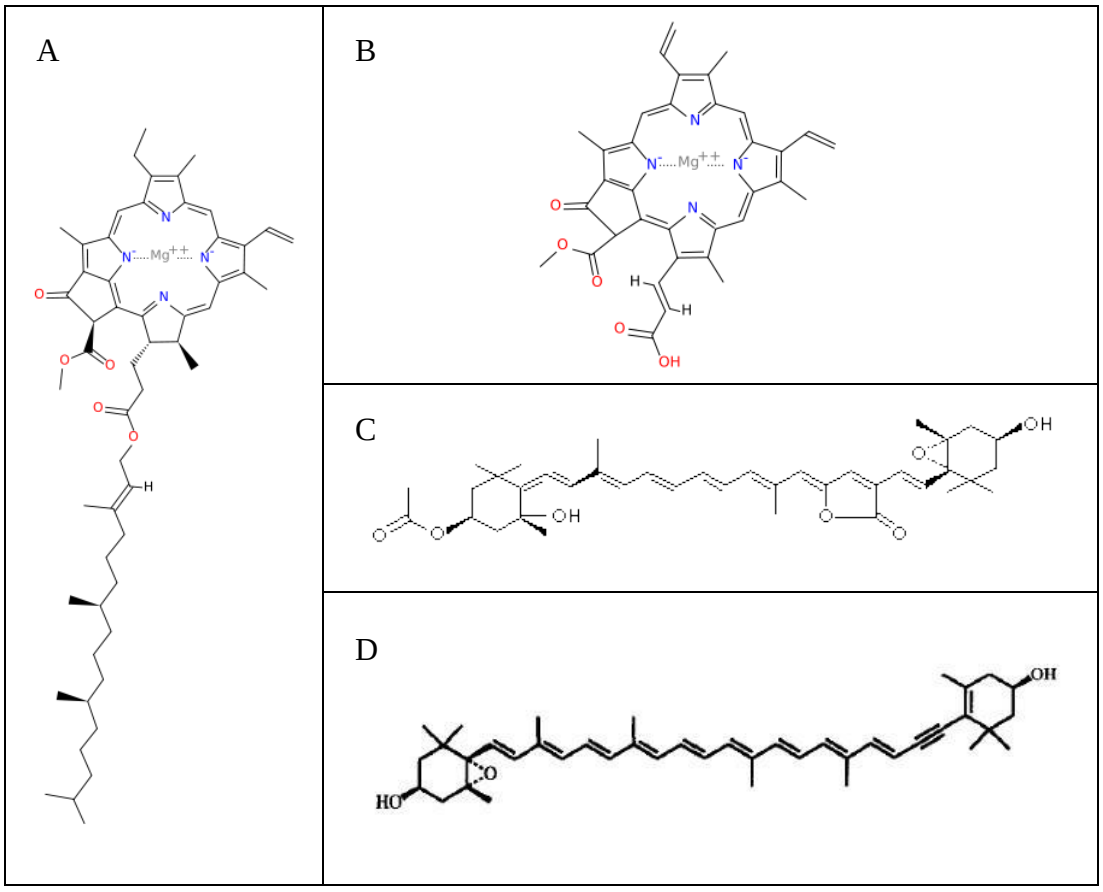

Figure 3: Pigments in PDCP: A – Chl *a*; B – Chl *c*; C – peridinin; D – diadinoxanthin.

Two different procedures (including two different detergents) were employed to identify the number of pigments in PDCP. The numbers corresponded in all cases, except for peridinin (see Table 2). Furthermore, two unidentified carotenoids were present in low amounts regardless to the method used. However, the number of pigments seems to be unrealistically high compared to closely related LHCs. This is supported by the finding that no significant red shift of Chl *a* Q_y band due to excitonic interactions was observed (Polívka et al. 2006).

[15] Two kinds of Chl *c* exist. PDCP contains Chl c_2. Nevertheless, because no other form of Chl *c* is mentioned in the text, the simplified abbreviation Chl *c* is used instead of Chl c_2.

PDCP is a member of the LHC superfamily. When compared with other LHCs (Hiller et al. 1995), there is a more significant identity towards the N-terminus of the proteins. However, the identity of 40% is in no case exceeded. It is not surprising that PDCP and Chl *b*-binding LHCs show less than 30% homology. On the other hand, the greatest identity is reached with fucoxanthin chlorophyll *a*/*c* protein (FCP), which has a very similar pigment composition as PDCP: fucoxanthin (a carbonyl carotenoid), diadinoxanthin, Chl *a*, and Chl *c*.

As can be seen in the AS of PDCP (Fig. 4), features belonging to Chls dominate. In the red part of the spectrum peaks the Chl *a* Q_y band. Smaller bands appear below 660 nm where Q_y band of Chl *c* coincides with the higher vibrational bands of Chl *a*. Further to blue, the influence of carotenoids increases. The shoulder around 540 nm is attributed to peridinin, and the one around 495 nm to diadinoxanthin (Polívka et al. 2006). In the blue part of the spectrum, Soret bands of Chls stick out, at 458 nm (Chl *c*) and 440 nm (Chl *a*).

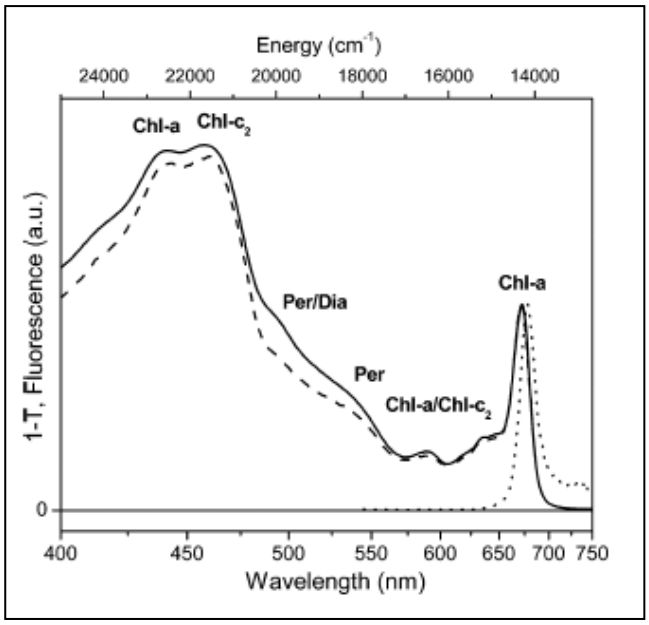

Figure 4 (Polívka et al. 2006): Absorption (solid line), emission (dotted line), and fluorescence excitation (dashed line) spectra of PDCP.

The emission spectrum of PDCP (Fig. 4) is dominated by the peak of Chl *a* fluorescence at 678 nm, and further to red accompanied by the vibrational band of the same pigment at 740 nm. Similarly as in PCP, a very high efficiency of energy transfer (Per-Chl *a*, Chl *c*-Chl *a*) was demonstrated using fluorescence excitation spectroscopy (Fig. 4). Nevertheless, the about 90% peridinin-Chl *a* energy transfer efficiency is restricted to the region from 530 to 550 nm while it decreases for wavelengths below 525 nm. This phenomenon might be caused by the other carotenoid, diadinoxanthin, possibly having the photoprotective role. Chl *c*-Chl *a* energy transfer efficiency amounts almost 100%, as demonstrated in the 550-680 nm region of the fluorescence excitation spectrum.

Pump-probe spectroscopy provided further insight into the energy transfer pathways within PDCP (Polívka et al. 2006). In this study, transient absorption data recorded after excitation at two different wavelengths (540 nm and 500 nm) are presented. One of the differences between the spectra at 3 ps was that a new band around 540 nm appeared after 500-nm excitation while after 540-nm excitation no similar feature was detected. This band was ascribed to diadinoxanthin, which was excited together with peridinin at 500 nm, but was not at 540 nm. From further analyses of these spectra and

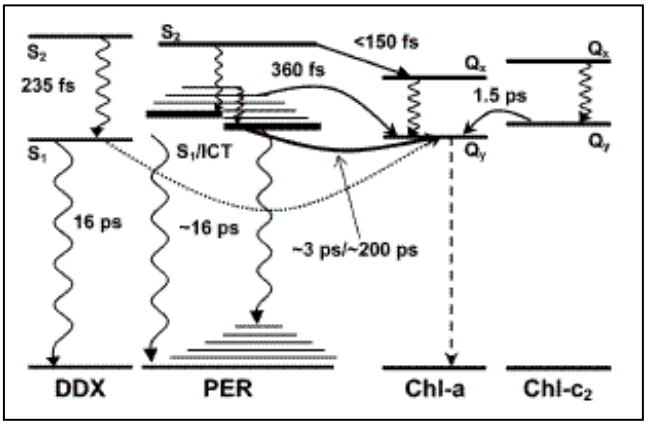

Figure 5 (Polívka et al. 2006): Energy transfer pathways in PDCP; DDX – diadinoxanthin; PER – peridinin.

other measurements, a model of energy transfer pathways was constructed (Fig. 5). The main energy transfer channel to Chl *a* proceeds via the S_1/ICT state of peridinin (including the vibrationally hot S_1/ICT), which has a significant CT character. This channel operates with energy transfer efficiency reaching almost 100%. Another channel is via S_2 state of peridinin with efficiency 25-50%. The uncertainty in determination of the efficiency follows from the fact that the energy transfer via the S_2 state proceeds on the sub-150-fs time scale, which is beyond the limits of time resolution of the used apparatus. Among others, from the extreme rate of energy transfer from S_2 follows that S_2 state of diadinoxanthin cannot be involved in this energy transfer because its lifetime in PDCP was assigned to be 230 fs. Similarly, no additional Chl *a* bleaching was recorded after disappearing of the above mentioned 540-nm band, resulting in the assertion that even S_1 state of diadinoxanthin is not involved in energy transfer to Chl *a*. Consequently, the role of diadinoxanthin was assigned to be photoprotection. The last important energy transport channel is the one from Chl *c* to Chl *a*, characterized by the time constant of 1.5 ps.

Nevertheless, many questions still remain unanswered. Any predictions are not easy to confirm because of unknown structure and even exact pigment composition of PDCP (Hiller et al. 1993). This thesis is thus focused on deepening our knowledge of PDCP. In particular, series of measurements varying in excitation wavelengths covering almost the whole blue-green region was performed. As a result, different involvement of particular carotenoid species should be revealed.

2. MATERIALS AND METHODS

2.1 Sample preparation

It should be mentioned that sample preparation was not the subject of this thesis. Thus only brief overview of the preparation process, according to Polívka et al. (2006), will be presented here.

After harvesting and cell disintegrating of algae of the species *Amphidinium carterae* (in detail described by Sharples et al. 1996), two washing steps were performed to remove PCP and other water-soluble proteins. The top layer of precipitated membranes was washed with a buffer at pH 7.5, and re-suspended in the same buffer. To release the pigment proteins from non-polar interactions with membrane lipids, 10% detergent β-dodecyl maltoside was added, and the solution was stirred in the dark at 4 ºC for 2 h. Consequently, centrifugation at 39 000 *g* was performed, followed by loading the supernatant onto the 5-40% linear sucrose gradient made in the previously used buffer and centrifuging at 200 000 *g* for 18 h. PDCP was then located within the band of 5-10% sucrose. The middle of the band was collected, dissolved in a buffer (25 mM Tris at pH 7.5, 2 mM KCl), and stored in the dark at -80 ºC.

Prior to the measurements, PDCP sample was thawed and diluted to reach the optical density of about 0.45/mm at 672 nm (Q_y band of Chl *a*). The solution was then transferred into the rotational cuvette. Such a cuvette consists of two round quartz glasses (1-mm front window and 2-mm back window), between which a 1-mm Teflon spacer is placed, forming the volume of about 1 ml into that approximately 700 µl of the sample is pipetted. All these parts are embedded in a metal fixture, leaving the sample space uncovered. By rotating the cuvette during the pump-probe measurement at sufficient frequency, experimental conditions under which every pump pulse hits a fresh sample is reached.

2.2 Time-resolved spectroscopy

In general, time-resolved spectroscopy is any study which employs electromagnetic radiation to investigate dynamic processes. Implementation of this method in the visible region was greatly enhanced after pulsed lasers became available. Femtosecond time-resolved spectroscopy has currently become quite a routine technique. Moreover, even attosecond[16] pulses have already been reported. Nevertheless, they have a broad spectrum reaching at least 200 nm for a 1-fs pulse with central

[16] These are slightly misleading names for ultrashort pulses; when attosecond pulses are mentioned, it is often thought that such pulses are shorter than a femtosecond, i.e. the attosecond pulse's length is usually hundreds of attoseconds. Similarly, femtosecond pulses have most often the duration of at least tens of femtoseconds.

wavelength in the middle of the visible region, which results from the energy-time uncertainty relation ($\Delta E \Delta t \geq \hbar$) . This makes them unusable for many studies because selective excitation is most often required.

There are differences in the architecture of particular experimental setups. I will more thoroughly describe the one called *pump-probe* technique (alternatively called *transient absorption spectroscopy*)[17] using visible light. This method with ~130-fs time resolution was employed in measurements presented in this thesis.

2.2.1 Pump-probe spectroscopy

The principle of this method is as follows (Fig. 6): a laser (1) produces ultrashort monochromatic pulses forming a beam (red), which is then split into two. The one forms the excitation beam ("pump" – green), and the required frequency is reached in the light converter (2). The other passes through a medium (3) in which a white light beam ("probe" - white) is produced. Both beams go through the sample (5). To study the time evolution of the photoinduced absorption changes within

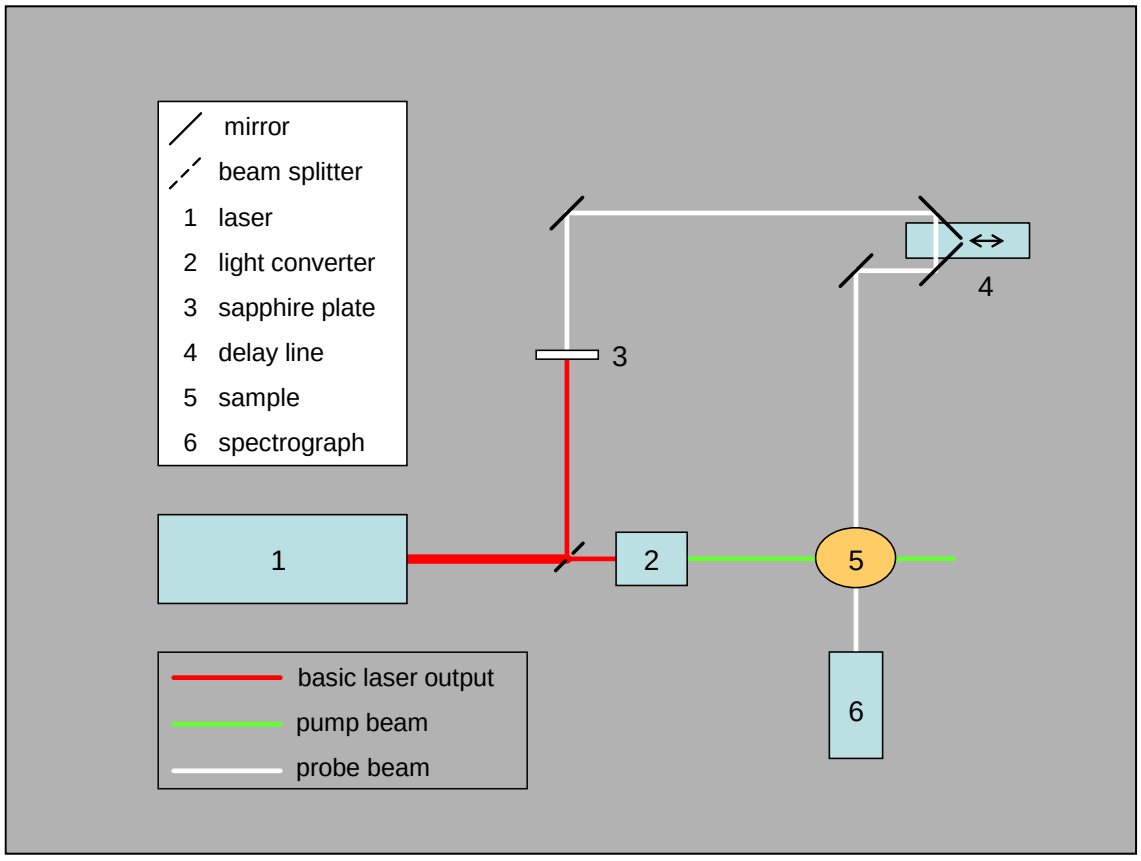

Figure 6: Setup for the pump-probe experiment. Details are given in the text.

[17] It should be mentioned that there is a difference between the terms (i.e. not between the techniques alone) *pump-probe* and *transient absorption spectroscopy*. The former is related to the architecture of the experiment while latter rather refers to the result of the measurement, i.e. the spectra.

the sample, the delay between pump and probe progressively increases. The time difference is reached by letting the probe experience longer path than does the pump. The time delay Δt can be calculated as follows: $\Delta t = \frac{\Delta l}{v} = \frac{n(l_2 - l_1)}{c}$, where v is the speed of light in a particular medium, n the refractive index of the medium, c the speed of light in vacuum, l_1 and l_2 are lengths of trajectories of pump and probe, respectively, and Δl is their difference. Thus Δt of 1 ps corresponds to Δl of ~0.3 mm. Technically, this is achieved by operating of the appliance called *delay line* (4). It is a corner reflector, which is moved by means of a stepper motor. Finally, after pump and probe, respectively, go through the sample (5), the probe continues further to the spectrograph (6), where the light signal is dispersed by a diffraction grating onto the surface of the diode array, and converted into the electric signal. Afterwards, such a signal is digitized so that it can be processed by a computer.

A phenomenon called *chirp*, which is an unwanted by-product of the use of optical components in the pathway of the probe, should also be mentioned in this section. Due to dispersion, blue part of the spectrum is delayed more than the red one when a polychromatic pulse (i.e. probe) travels through a medium with the refractive index *n*. Consequently, the chirp is strong when the probe pulse goes through optical components with high values of *n* (lenses, filters etc.). To minimize the effect of the chirp, the use of optical components such as filters should be minimized; alternatively, in some cases, conventional optics can be replaced by more sophisticated components (e.g. lenses by spherical mirrors).

The usability of the pump-probe spectroscopy will be explained in the following section. Its basic purpose is to study excited-state dynamics of molecules, but many other conclusions can be inferred out of it (e.g. energy and electron transfer processes). First, the pump goes through the sample. When there is a molecule with energy of an allowed transition corresponding to the energy of the incident photons, the absorption occurs. After time Δt, which is set by the delay line, the probe pulse is applied, resulting in another process, e.g. absorption from an excited state, which is called *excited state absorption* (ESA; Figs. 7C, 7D). On the other hand, negative signal can be recorded, which is called *bleaching and/or stimulated emission* (Fig 7C). Bleaching is created because excited molecules "are missing" in the ground state, so the transient absorption in the region of steady-state absorption is smaller compared to the reference. The other source of negative signal is stimulated emission. In this case, some photons from the probe "force" the molecules to depopulate the excited state. The process is accompanied by emitting photons with energy of the involved transition, resulting again in negative signal.

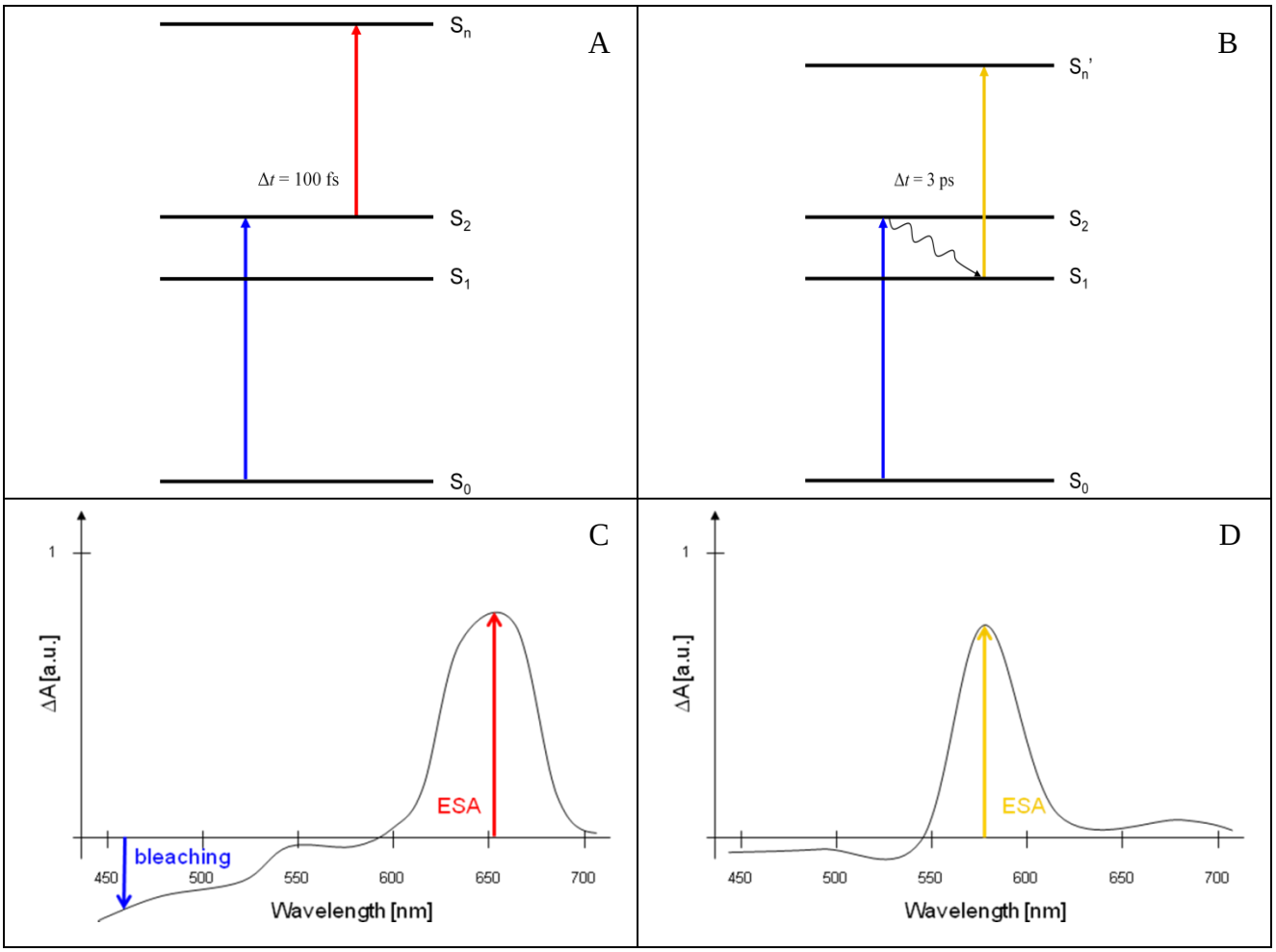

Figure 7: A, B – energy state diagram of a molecule with depicted transitions differing in time delay between pump (blue arrow) and probe pulses (only the absorbed wavelengths, symbolized by red and yellow arrows, are shown). C – TAS corresponding with A; D – TAS corresponding with B.

The motivation to use this technique lies in the fact that the time Δt increases, so information about the dynamics can be obtained. For instance, let us assume that a molecule was excited into the S_2 state (Fig. 7A). The S_2 lifetime is about 200 fs, so when Δt is 100 fs, the molecule is probably still in the S_2 state and the transient absorption spectrum (TAS) reflects ESA from the S_2 state, which is schematically shown in Figure 7C. Nevertheless, when the time Δt is 3 ps, the molecule has already made a transition into a lower state, for example into S_1 (Fig. 7B). Consequently, the shape of the TAS changes because the S_1 state possesses different spectroscopic properties (Fig. 7D). By systematic scanning the spectra with increasing Δt, we can obtain a lot of information about excited states of a molecule. The result of a measurement is thus a matrix where a particular transient absorption signal is determined by two quantities - wavelength (λ_{trans}) and Δt. Figures 7C and 7D show spectral sections of this matrix, which is quite a usual way of demonstrating of data.

The example introduced in the previous paragraph was quite simple because only one kind of molecules was present in that virtual experiment. Consequently, interpretation of data obtained from

such an experiment is sometimes straightforward. However, when e.g. light harvesting complexes (containing many chromophores in protein environment) are studied, the interpretation of data is significantly more complicated, but thorough analysis can provide valuable information because studies of such systems reflect the native state to some extent.

2.2.2 Experimental setup

The experimental setup used for measurements presented in this thesis is depicted in Figure 8. The crucial component is the laser system Integra-I (Quantronix) providing 790-nm pulses of ~130 fs duration at a repetition rate of 1 kHz (1). The spectral width of the pulses due to the energy-time uncertainty relation is at least 2.5 nm for the wavelength of 790 nm. The duration of pulses also represents the time resolution of the system. The output of the laser is split into pump and probe pulses[18].

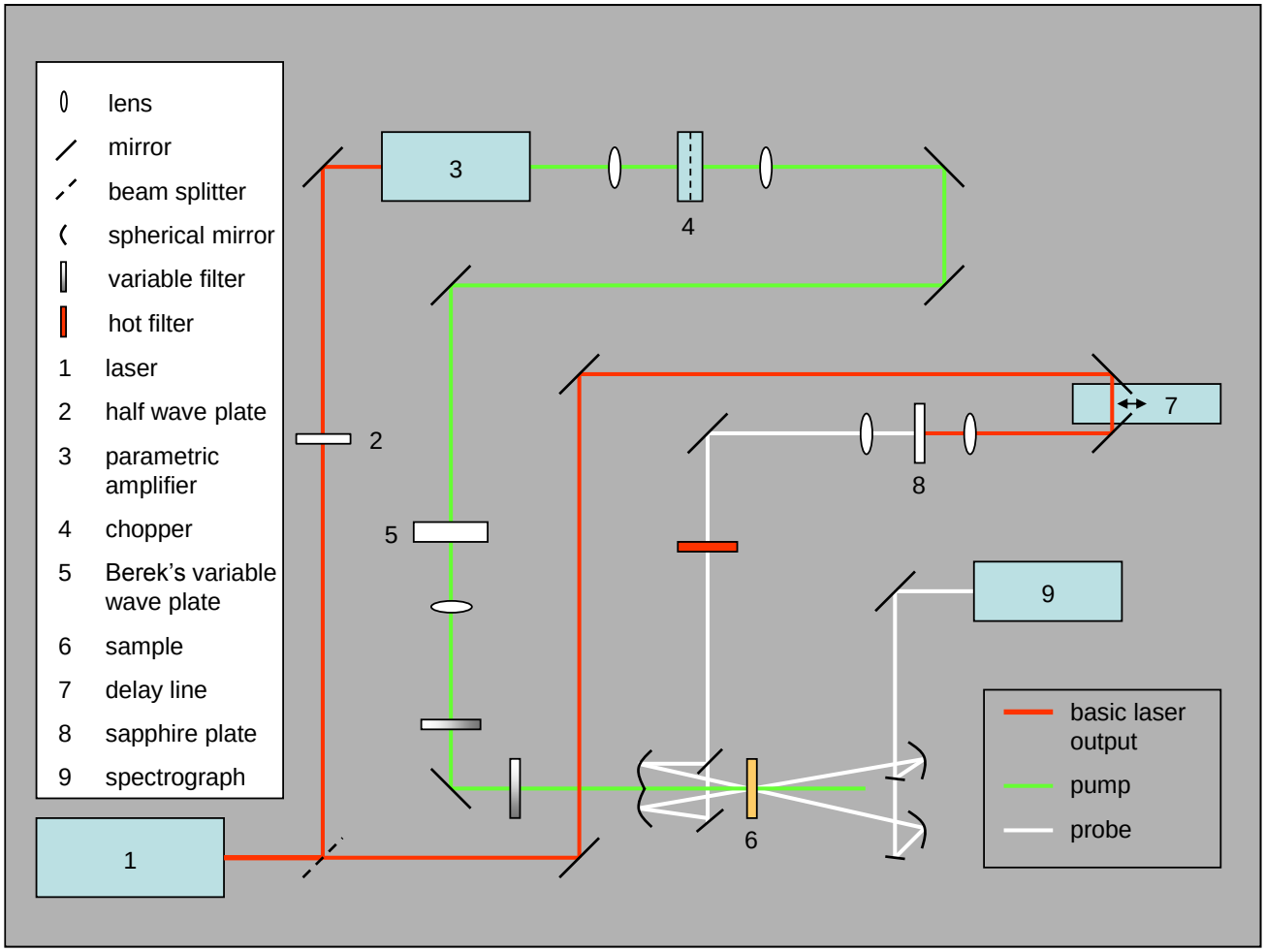

Figure 8: Experimental setup for the pump-probe measurement. Details are given in the text.

[18] Another possibility is to consider the beam as pump after leaving the light converter, and probe after leaving the crystal. This approach is used in Figure 8.

Initially, we will trace the pathway of the pump[19]. The first optical component is a *half wave plate* (2), which changes the original vertical polarization of the Integra output to the horizontal one that is necessary for other optical components. The turn of the polarization is achieved by a birefringent material, in which the refractive indexes for the ordinary and extraordinary beam differ, thus producing the phase delay. This, for half-wavelength thickness of the crystal, results in rotation of the linearly polarized light about 90º. The parametric amplifier TOPAS (Light Conversion) is used to generate and amplify the desired wavelength of the pump (3). This is achieved by means of nonlinear effects. The pump (only a small portion of the initial intensity) enters the nonlinear crystal, and the seed, i.e. signal and idler, originates in the process called optical parametric generation. By rotating the crystal it is possible to adjust the frequencies of signal and idler, providing the energy conservation law is satisfied: $\omega_p = \omega_s + \omega_i$; ω_p, ω_s, and ω_i are frequencies of the pump, signal, and idler, respectively. Consequently, the seed is spectrally narrowed and pre-amplified. The latter operation is again achieved in the same crystal after both the seed and another small portion of pump enter it. The other step is to amplify the seed with most of the pump. Finally, at the output, additional crystals enable, by sum, difference, and higher harmonic generation, tuning to almost any wavelength in the range 200-20000 nm. Another component in the pump pathway is the *chopper* (4) that filters every second pump pulse. Thus when the laser operates with the frequency of 1 kHz, the chopper's frequency is set to 0.5 kHz. This arrangement enables to filter out the intensity fluctuations proceeding on longer time scale. To further increase the signal-to-noise ratio, more measurements at each time delay are carried out and averaged. The next element of the setup is the *Berek's variable wave plate* (5). The birefringent crystal is adjustable in two ways – it can be tilted and/or rotated around the axis of birefringence. By setting of these two independent parameters it is possible to reach the desired polarization (for wavelengths in the range 200-1600 nm), which for standard measurements is set to the magic angle (54.7º) ensuring that anisotropy effects do not play any role. The destination for the pump beam is the cuvette with the sample (6), where it excites the studied molecules. It is important to prevent the pump pulse from entering the spectrograph because it would interfere with the probe signal.

Let us examine the way of the probe pulse. The probe first goes to the delay line (7), which sets the appropriate time delay between pump and probe. Next it is led through the crucial component – a sapphire plate (8), in which white light continuum is produced by means of nonlinear effects. The hot filter placed behind the sapphire plate eliminates the residual basic frequency. Before entering the sample space, the probe pulse is divided into reference and probe (see Fig. 9) that are focused to

[19] Optical elements such as filters and lenses are omitted in the text, but depicted in the accompanying scheme.

the sample using the spherical mirrors to avoid additional chirp. Finally, both beams are led to the spectrograph (9), where they are, by means of a grating, dispersed on two separate diode arrays, each consisting of 1024 diodes. After digitization, the signal proceeds into the computer. A special program calculates the transient absorption (accompanied by spectral and temporal characterization), and enables to extract these data as a matrix for further processing.

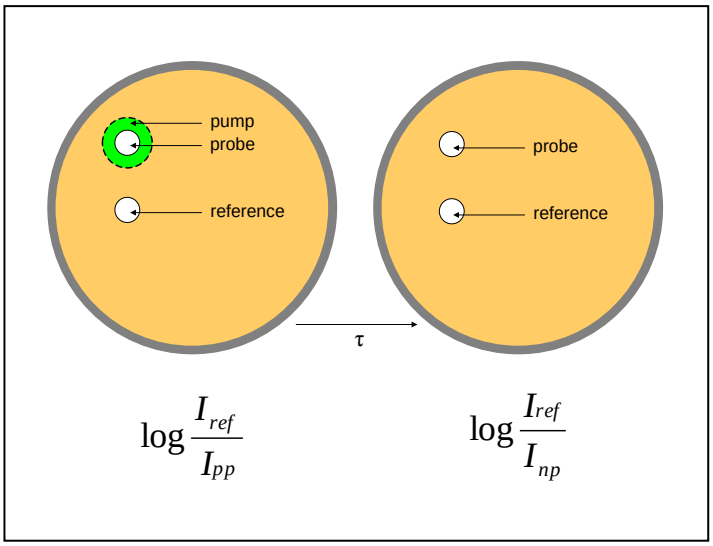

Figure 9: Left part – pump-ON measurement: the cuvette is initially illuminated by pump, and, after time Δt set by the delay line, probe and reference pulses are simultaneously applied. Right part – pump-OFF measurement: after time τ given by the laser's repetition rate, the same as in the left part happens except that the probe is not pre-pumped.

Transient absorption (*TA*) signal is calculated using the following expression (Fig. 9): $TA = \log \frac{I_{ref}}{I_{pp}} - \log \frac{I_{ref}}{I_{np}}$; I_{pp} and I_{np} are intensities of probe with (pump-ON) and without (pump-OFF) previous illumination by pump, respectively, and I_{ref} is the intensity of reference. Chopper in the pathway of the pump enables separation of pump-ON and pump-OFF measurements, the time delay between them being denoted as τ in Figure 9. The expression $\log \frac{I_{ref}}{I_{np}}$ should be equal to zero under ideal conditions, but in case of long-term instabilities it helps to increase the signal-to-noise ratio.

2.3 Parameters of experiments

The description of the experiments will be presented in this section. All experiments were performed using the apparatus described in section 2.2.2. The plan was to employ pump-probe technique for the wide-range study of energy transfer pathways in PDCP. Eleven different excitation wavelengths were applied as depicted in Figure 10 in section 3.1. Here are the most important steps preceding each measurement with new excitation wavelength:

- The new excitation wavelength was set using the parametric amplifier TOPAS.
- The accuracy of the pathway of the pump pulse was checked and adjusted.
- Because the setting of the Berek's variable wave plate is wavelength-dependent, the polarization of pump (magic angle with respect to probe) was also checked and, if needed, adjusted.

- The overlap of the pump and probe in the sample space was controlled.
- The excitation intensity was measured. In this study, the correct reading of the excitation intensity is crucial because it serves as a normalization factor enabling the comparison of data obtained from measurements using different excitation wavelengths. In none of the experiments the energy exceeded 2 μJ per pump pulse. The spot of the pump pulse in the sample had the diameter ~0.5 mm, so the photon flux density was always below 3.10^{15} photons.cm^{-2}.

AS were measured to find out the level of sample degradation. Comparing the spectra before measurements and after them, the decrease of the signal did not exceed 10%.

2.4 Transient excitation spectra

As mentioned above, more excitation wavelengths were used to study energy transfers in PDCP. Such an approach enabled to develop a novel way of interpretation of these data, which is called transient excitation spectra (TES). A parallel can be drawn between TES and fluorescence excitation spectra. As in the latter mentioned method, in case of TES the excitation wavelength represents the x-axis (see Fig. 13). In contrast, the *TA* signal normalized to the excitation intensity appears on the y-axis in the TES. The expected merit of this method lies in the fact that we have two variables (i.e. the wavelength of the particular transient absorption signal, $\lambda_{trans,}$ and the corresponding time delay between pump and probe, Δt) to choose for each point in the TES. In particular, in case we know an ESA band of a carotenoid and the lifetime of the corresponding excited state (from measurements on the pure carotenoid in solution or in a different simpler pigment-protein complex), we should be able to extract the information about the carotenoid, and consequently its involvement in processes varying with excitation wavelength. Nevertheless, two carotenoids with very similar spectral-temporal properties cannot be distinguished.

2.5 Global fitting

All data were analyzed globally (van Stokkum et al. 2004) using commercially available software DAFit (Pascher Instruments). Such treatment involves three main stages[20]. First, the procedure involves chirp correction of data. Second, deconvolution of the instrument response function, fitted as a Gaussian, is performed. Third, a sequential model is applied resulting in a set of evolution-associated difference spectra (EADS).

[20] This is meant from point of view of a principle (not what the user is to do with the program).

The sequential model, into which the data are fitted, is predefined in the fitting program, and is formed by a limited number of spectral components (“states”) evolving one into another with time. Thus the first EADS decays with the first lifetime; the second EADS is formed with the first lifetime, and decays with the second lifetime etc. Although this approach enables to trace the spectral evolution of the system, the individual components do not necessarily correspond to pure excited states. Such situation arises when a branching process is present, e.g. when an excited state decays into two lower states. Consequently, the EADS after the branching represents a mixture of the spectra of the two lower-lying excited states. To overcome problems with the branching processes, more sophisticated method must be applied (target analysis), but it was not used in the study presented here.

3. RESULTS AND DISCUSSION

3.1 Steady-state spectroscopy

Although steady-state spectroscopic data of PDCP have already been described (Polívka et al. 2006), the PDCP sample studied here exhibited some differences. Its AS is shown in Figure 10[21]. The important distinctions are as follows: 1) the hypothesized shoulder around 495 nm, attributed by Polívka et al. (2006) to diadinoxanthin, is not that pronounced in the PDCP sample used for this study; 2) when compared quantitatively, both Soret and Q_y bands are less intensive in our sample. Thus it can be concluded that on average fewer Chl molecules per one protein complex occur in PDCP studied here. In addition, this tendency is probably even more expressed for Chl *a*. This can be inferred from bigger difference between peaks of Chl *c* (458 nm) and Chl *a* (440 nm) in the Soret region compared to the same feature in Figure 4. Consequently, the pigment composition of the individual sample probably depends on cultivation conditions and/or the sample preparation process.

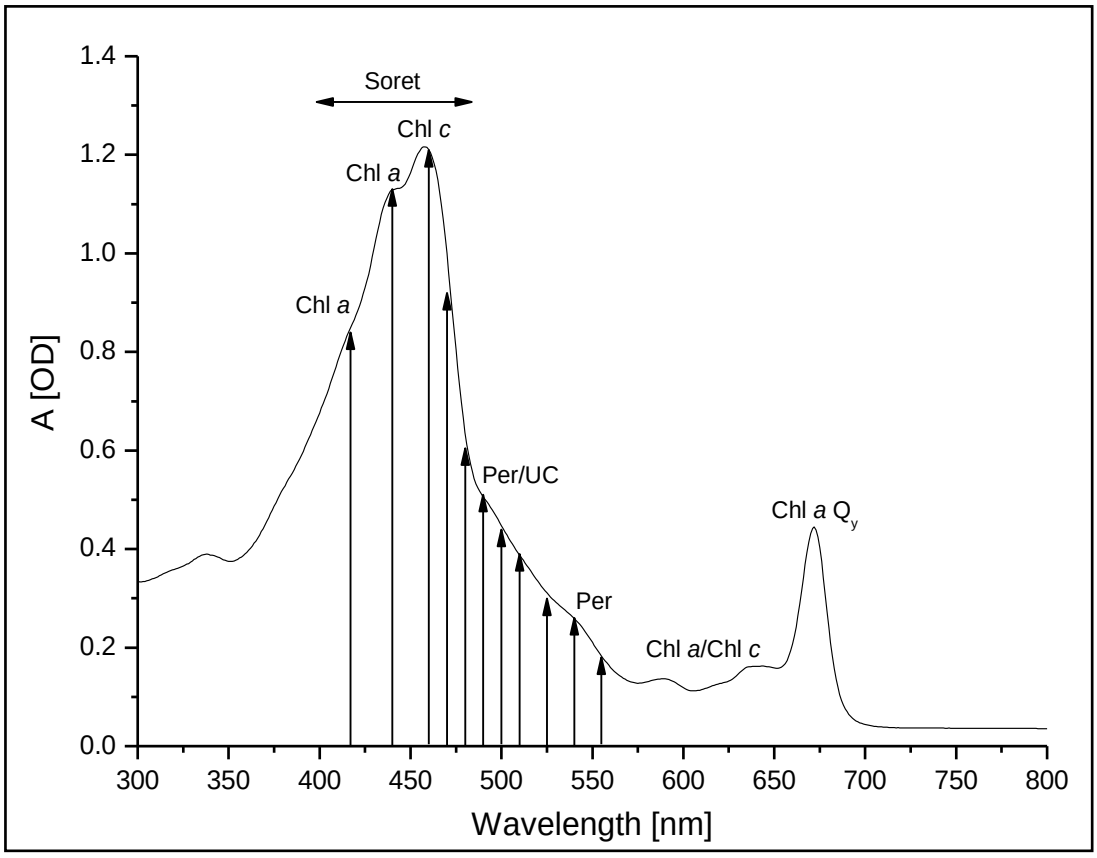

Figure 10: Absorption spectrum of PDCP. Arrows show the eleven applied excitation wavelengths: 417, 440, 460, 470, 480, 490, 500, 510, 525, 540, and 555 nm. Distinct features are ascribed to particular pigments (Per = peridinin, UC = unidentified carotenoid (introduced below)).

[21] Furthermore, Figure 10 shows which excitation wavelengths were applied (see section 2.3 for description).

3.2 Pump-probe spectroscopy

3.2.1 Transient absorption spectra

Figure 11 shows TAS recorded after excitations at 440 nm, 480 nm, and 540 nm (see also Fig. 10). These excitation wavelengths were chosen as typical representatives because different pigments contribute to the signals. For each case, five spectra differing in time delay Δt are shown (200 fs, 500 fs, 3 ps, 10 ps, and 50 ps). All spectra are normalized to the excitation intensity to enable the comparison of the strength of signals for different excitation wavelengths. Important features of the spectra will be described in the next paragraphs.

The 440-nm excitation (Fig. 11A) matches the strong absorption of Chls. The TAS consist of a wide-range multi-shoulder ESA and a noticeable dip around 674 nm caused by the Chl *a* bleaching. The dip is already present in the shortest Δt of 200 fs,[22] indicating that direct excitation into the Soret region of Chl *a* occurs. Nevertheless, the deepening of the Chl *a* bleaching continues also in later times. Because carotenoids absorb in the region of excitation, both the fast energy transfer from peridinin S_2 state (taking place on <150 fs time scale according to Polívka et al. 2006) and the slower transfer from (hot) S_1/ICT[23] to Chl *a* may contribute to the growth of the bleaching. Against the assumption that carotenoids significantly absorb (and consequently transfer energy) after 440-nm excitation rises the fact that no ground-state bleaching is present in the spectra, but this might be caused by the fact that it occurs deeper in blue, i.e. out of the spectral window. To complete the list of the possible energy pathways after 440-nm excitation, the absorption of Chl *c* also occurs, enabling energy transfer to Chl *a* because the Q_y state of Chl *c* is higher than that of Chl *a* (see Fig. 5). Because a hint of bleaching indeed appears around 645 nm (matching the expected Chl *c* bleaching), this energy transfer channel is likely active. Finally, it should be emphasized that the Chl *a* bleaching is more intensive after 10 ps than after 50 ps. It would be tempting to explain this phenomenon as back energy transfer from Chl *a* to carotenoids, thus confirming the quenching role of carotenoids. However, equilibration/annihilation processes (van Grondelle 1985) are most likely the reason of the observed long-time dynamics of the Chl *a* bleaching. When intense pulses are used, it is more probable to excite adjacent Chls in one complex. Consequently, it is possible that one Chl transfers its excitation energy into another, yet not relaxed, Chl molecule. The former thus reached the ground state, and the latter was promoted into a higher excited state that subsequently relaxes

[22] No certain conclusions can be inferred from spectra at such short Δt because tracing of very fast processes is impossible due to insufficient time resolution.

[23] For accuracy, those two mentioned processes do not follow the same pattern. The former transition proceeds from S_2 state of peridinin probably to Q_x state while the latter from (hot) S_1/ICT state to Q_y state of Chl *a*. Nevertheless, both of them express as Chl *a* bleaching signal, but on different time scales.

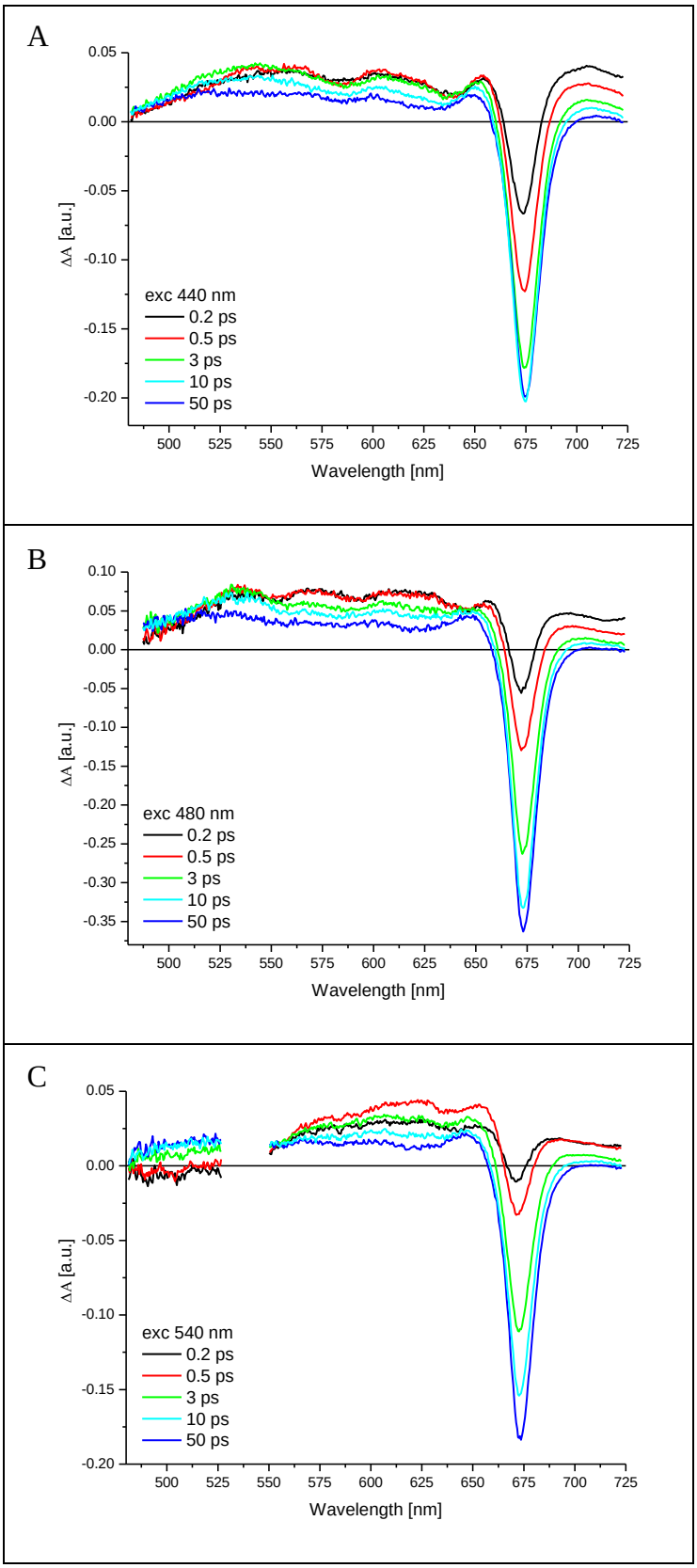

Figure 11: TAS after excitations at 440 nm (A), 480 nm (B), and 540 nm (C); exc = excitation wavelength. Data were normalized to the excitation intensity.

quickly back to the lowest excited state via internal conversion, resulting in decrease of the initial bleaching signal.

The situation after 480-nm excitation is rather different (Fig. 11B). Here both carotenoids are excited, i.e. peridinin and diadinoxanthin. Furthermore, Chl *c* might be excited. The main difference, compared to the excitation at 440 nm, is the better pronounced ESA band centred around 530 nm. Polívka et al. (2006) ascribed this band to diadinoxanthin, although this assignment may be challenged on the basis of the data presented here. The signal at 530 nm is comparably strong as the broad ESA around 610 nm assigned to peridinin (Zigmantas et al. 2001). Taken into account the peridinin/diadinoxanthin stoichiometric ratio (Hiller et al. 1993), the intensity of signal emanating solely from diadinoxanthin seems to be unrealistically high. The 530-nm band alone is remarkable because it is slightly blue-shifted (systematically, i.e. for most of the excitation wavelengths) compared to the band recorded by Polívka et al. (2006)[24], which could support the assumption that the pigment composition of PDCP sample could be slightly different here (see section 3.1 and 3.3). However, regardless to the compound involved, it seems

[24] Another difference is the comparable intensity of 530-nm and 610-nm signal recorded here. Measurements conducted by Polívka et al. (2006) showed the 610-nm band to be more intense for short Δt (for 500-nm excitation).

unlikely that signal around 530 nm should be associated with diadinoxanthin occurring in PDCP in such small amounts. Thus having challenged the assignment of the 530-nm band to diadinoxanthin, when discussing the origin of the 530-nm band, the term *unidentified carotenoid* (UC) will be used. A feature accompanying the excitation of carotenoids is the ground state bleaching present in the blue part of the TAS at early times. However, the bluest region of the TAS had to be omitted because of strong contamination by the scattering of excitation light. The broad ESA band above 600 nm and that one around 565 nm relate to S_1/ICT-S_N transition of peridinin (Zigmantas 2001). Chl *a* bleaching again appears already at the early time of 200 fs. Here, compared to the excitation at 440 nm, the onset of the Chl *a* bleaching is at least to some extent caused by fast energy transfer from the peridinin S_2 state to Chl *a*. As Δt progresses, the Chl *a* bleaching deepens, indicating energy transfer from (hot) S_1/ICT state of peridinin. The dip around 645 nm can be again assigned to Chl *c* that is also directly excited at 480 nm. The Chl *c* bleaching signal disappears within 3 ps, which is in agreement with time constant of energy transfer from Chl *c* to Chl *a* of 1.5 ps revealed by Polívka et al. (2006). Thus Chl *c* is the other important energy donor for Chl *a* (apart from peridinin).

Finally, spectra following the excitation at 540 nm (Fig. 11C) will be described. In this case, the major absorbing pigment is peridinin, which is confirmed by the presence of its typical spectral features. The other pigments, including the UC, have negligible absorption at 540 nm. At the shortest time delay, a weak ground-state bleaching in the blue-green part of the TAS is replaced by ESA from the S_1/ICT state in the "redder part" of the spectrum. The energy transfer from peridinin S_2 state is again active, which is demonstrated by the early Chl *a* bleaching. With continuing depopulation of the peridinin S_2 and hot S_1/ICT state raises the ESA associated with S_1/ICT-S_N transition (200 fs – 500 fs), and Chl *a* bleaching deepens. During the next step (500 fs – 3 ps) the ESA signal decreases, which is followed by strong deepening of Chl *a* bleaching indicating intensive peridinin-Chl *a* energy transfer, which continues, although not to such a large extent, during the other steps. The initial ground state bleaching is replaced by weak ESA for longer delays. No ESA around 530 nm is present in any spectrum after 540-nm excitation meaning that the AS of the UC is blue-shifted compared to peridinin. TAS obtained after 540-nm excitation match well those published by Polívka et al. (2006) (for the same excitation wavelength).

The uncertainty in determination which pigment is excited by the particular wavelength should be discussed here. Although we know the behaviour of many carotenoids in solution, it is still insufficient because the protein acts not only by its polarity and other properties, but also by non-covalent bonds with pigments (see section 1.2). CCs are known for their sensitivity to polar environment in solution, but changes in spectroscopic properties caused by protein environment must be even more dramatic, which can be demonstrated by the presence of peridinin response also after excitations

at 540 and 555 nm. Even in polar methanol, the absorption of peridinin at these wavelengths is rather weak (Zigmantas et al. 2001). Fucoxanthin, another CC, is also considerably red shifted in FCP compared to when dissolved in polar methanol (see Fig. 1 in Papagiannakis et al. 2005). The situation is further complicated by proposed blue-shifted and poorly transferring carotenoids present in LHCs (Damjanović et al. 2000), which, as will be mentioned later, might be also the case of peridinin in PDCP. It is clear from the above-mentioned examples that each kind of LHC is unique, so we cannot be absolutely sure which pigments will be excited by a particular excitation wavelength.

3.2.2 Kinetics

Figure 12 displays kinetic traces (normalized to their maxima) in the spectral regions of interest (pigments contributing the most in each region are denoted in parentheses), i.e. signals around 530 (UC), 610 (peridinin), and 673 nm (Chl *a*). The kinetic traces are accompanied by corresponding fits that were obtained from global fitting analysis (section 3.4). Comparison of the kinetics is conducted for 440-, 480- and 540-nm excitations. Such representation enables to depict differences in temporal evolution of signals caused by changing excitation wavelength. Fits normalized to the excitation intensity are shown in the insets.

Global fitting analysis further revealed that the dynamics is governed by four (by five in cases of long-time evolution in the Chl region) time constants (attributed to particular processes according to Polívka et al. 2006): sub-0.1 ps (energy transfer from peridinin S_2 state to Chl *a*), 0.34 ps (energy transfer to Q_y of Chl *a* via hot S_1/ICT state), 2.1 ps (relaxed S_1/ICT-Chl *a* Q_y energy transfer), 15 ps (dynamics connected with the UC), and 200 ps (equilibration/annihilation processes). The involvement of these processes depends on both the applied excitation wavelength and the kind of dominantly excited pigments.

The signal of the UC, shown in Figure 12A, expresses similar behaviour for the 440- and 480-nm excitations. These decay traces are mainly governed by the 15-ps time constant. The 540-nm kinetic trace is completely different. Initial bleaching is replaced by rather constant ESA that decays very slowly. At 540 nm, excitation of the UC is not expected. Thus the low intensity of the *TA* signal (see the inset) at the probing wavelength characteristic of the UC is not surprising. Its initial part can be assigned to ground-state bleaching of peridinin, consecutively being replaced by a weak ESA most likely originating from Chl *a*.

Peridinin kinetic traces are shown in Figure 12B. Here, the 2.1-ps time constant is dominant. The slower 15-ps time constant is pronounced mainly for the 440-nm excitation. On the other hand, the 0.34-ps time constant is present – particularly for the 540-nm excitation.

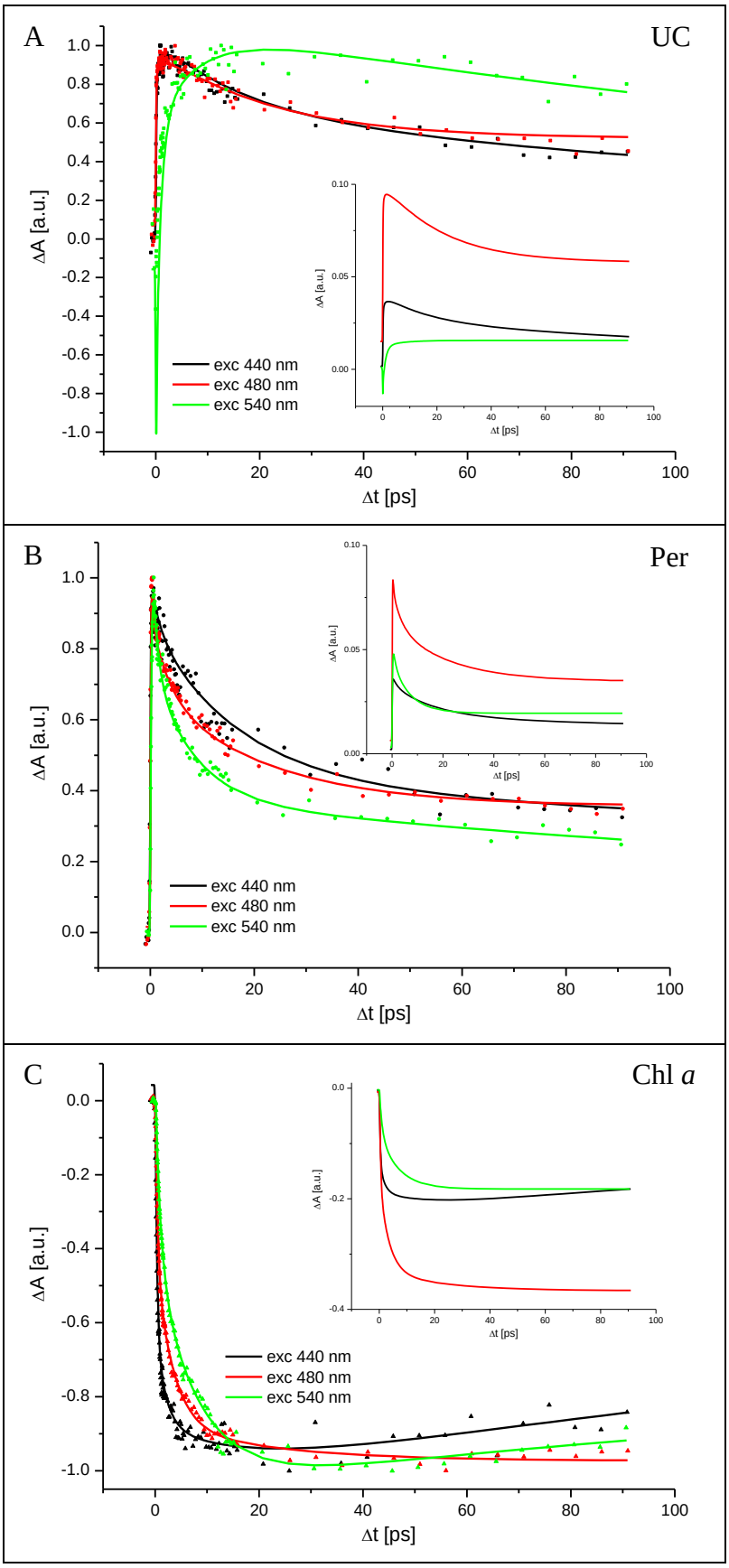

Figure 12: Kinetic traces of the unidentified carotenoid (A; squares), peridinin (B; dots), and Chl *a* (C; triangles) normalized to maxima of signals. Data are accompanied by corresponding fits. Fits normalized to the excitation intensity are shown in the insets.

The dynamics of the Chl *a* bleaching region is depicted in Figure 12C. Possible sub-100-fs processes, i.e. direct excitation of Chl *a*, fast Chl *c*-Chl *a* and peridinin S_2-Chl *a* energy transfers, are mostly pronounced for the 440-nm excitation. The involvement of the fast processes is less evident for the other two excitations, the least for the 540-nm. On the other hand, the slower time constants, i.e. the 0.34-ps and the 2.1-ps, become more pronounced with increasing excitation wavelength. The 440- and 540-nm excitations are remarkable for the long-time decay of Chl *a* bleaching even in the temporal window of our experiments (relating with the 200-ps time constant). This feature may be associated with the equilibration/annihilation processes (van Grondelle 1985).

Kinetic traces are also indicative of energy transfers between carotenoids and Chl *a*. The 15-ps component of the UC is not evident in the Chl *a* bleaching kinetics, so no energy transfer from the S_1 state of the UC to Chl *a* is expected. In contrast, peridinin is the energy donor for Chl *a*. This fact is best

pronounced for the 540-nm excitation where all pigments apart from peridinin absorb to a negligible extent. Here the peridinin decay nicely matches the growth of Chl *a* bleaching signal.

3.2.3 Transient excitation spectra

Constructing a TES is a new method of transient absorption data interpretation enabling extraction of characteristics of pigments. In particular, we aim here at separation of absorption profiles of peridinin and UC.

First, it is necessary to select states, spectral and temporal properties of which will be compared. Here, the states are S_1 of UC and S_1/ICT of peridinin. S_2 states are not suitable because their dynamics is inaccessible with the time resolution of the measurements.

Second, there are two variables which can be chosen (i.e. Δt and λ_{trans}) to extract the signals. As mentioned in section 2.4, spectral-temporal properties of the two molecules should be sufficiently different to ensure that we can reliably separate signals from the two pigments.

For peridinin in PDCP, the lifetime of S_1/ICT shorter than 3 ps was determined (Polívka et al. 2006). Because peridinin is excited directly, early Δt of 500 fs was chosen. The case of the UC is more complicated, but it is clear from Figures 11 and 12 that the signal associated with the UC has dynamics distinct from that of peridinin. Thus Δt of 10 ps was chosen as characteristic of UC because peridinin excited states are almost gone at 10 ps while the signal of the UC is still significant.

Molecular species	Peridinin	UC	Chl *a*
λ_{trans} [nm]	610	530	673
Δt [ps]	0.5	10	50

Table 3: Spectral and temporal regions of interest used for construction of TES.

The third distinct signal used for TES is Chl *a* bleaching around 673 nm. Chl *a* is the final acceptor of the excitation energy, and does not evolve significantly in the temporal window used in the measurements. Consequently, the Δt of 50 ps was chosen as the point of comparison with the other signals. Table 3 summarizes the spectral and temporal values used for construction of TES. To enable the comparison of data after different excitations, all signals were normalized to the excitation intensity. Error was set to 15% of the signal (the main contributor to the error is the fluctuation of the excitation intensity that cannot be determined with sufficient accuracy).

Figure 13A shows TES of peridinin, UC, and Chl *a*; Figure 13B displays only first two spectra in more detail. All TES can be divided into three parts – blue (for excitations from 417 to 460 nm),

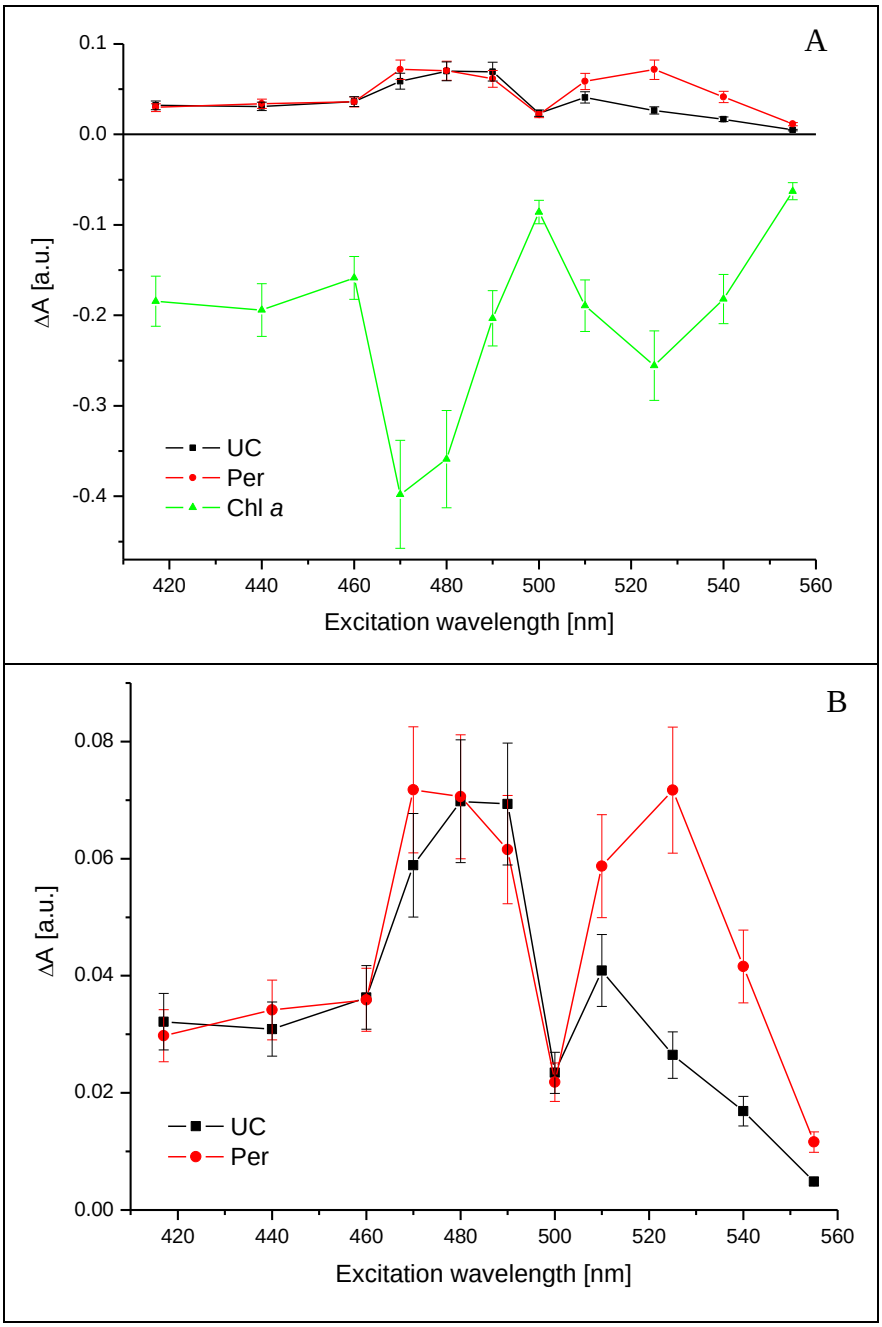

Figure 13: A – TES of the unidentified carotenoid, peridinin, and Chl *a* at regions defined in Table 3. B – TES of carotenoids in detail. Signals were normalized to the excitation intensity. Error was set to 15% of the signal.

middle (470 nm to 490 nm), and red part (510 to 540 nm), any of them possessing specific properties.

In the blue part the *TA* of carotenoids is rather weak, accompanied by relatively high magnitude of the Chl *a* bleaching (this fact is more obviously demonstrated in Fig. 14). The middle part contains signal from both carotenoid species, i.e. UC and peridinin. The highest value of Chl *a* bleaching is achieved for the 470-nm excitation. This region is overall characterized by strong Chl *a* bleaching, though with decreasing tendency toward red. In the red part of TES the peridinin signal dominates while the signal of the UC decreases[25]. The Chl *a* bleaching signal, similarly as in the middle part, to some extent reflects variations in *TA* of peridinin. The strength of the bleaching signal in the middle and red region demonstrates the vital importance of carotenoids for light harvesting. Rather outstanding are excitations at 500 and 555 nm. The origin of the intriguingly low signals after the 500-nm excitation is unknown. It must be noted, however, that very similar results were obtained in an independent measurement (data not

[25] This assertion may not be exact because the UC is probably not excited at least in case of the last three excitations (525, 540, and 555 nm). Thus, the signal at 530 nm for these mentioned excitations most probably originates mainly from Chl *a*. See Figure 11C or 12A where initial weak bleaching changes into weak ESA for longer Δt.

shown). The carotenoid signal following the 555-nm excitation is also rather weak, but this is expected for the red edge of TES because the absorbance at this wavelength is low (see Fig. 10).

Although the signal of carotenoids in the blue part of TES is not strong, the Chl *a* bleaching is quite intense. The reason for this behaviour lies most likely in the fact that significant part of the bleaching originates from direct excitation of Chls rather than energy transfer from carotenoids. This conclusion can be supported by the strong bleaching appearing already for very short Δt of 200 fs (see Fig. 11A). Even further increase of the bleaching signal can be in part associated with Chls, in particular with the Chl *c*-Chl *a* energy transfer. Nevertheless, peridinin-Chl energy transfer cannot be excluded.

Further insight into processes involved in the middle and red part of TES provides Figure 14, showing TES in which the peridinin signal was normalized to the bleaching signal for the 525-nm excitation. This normalization condition was chosen because the UC/peridinin *TA* signal ratio is here the lowest from all excitations. Thus comparison of the normalized peridinin signal and the Chl *a* bleaching might reveal whether peridinin is the dominant energy donor for all excitations. Higher magnitude of the peridinin signal compared to the bleaching signal indicates that not all energy from peridinin is transferred to Chl *a*; opposite case means that additional energy transfer channel is necessary. (It should be mentioned that this assumption is valid only if energy transfer efficiency is constant through the whole spectral region of TES). The TES in Figure 14 show that a good match of normalized peridinin and bleaching signals is reached for excitations from 490 to 525 nm. It would be tempting to explain the differences for the other excitations as a contribution of the UC to the energy transfer. Yet another hypothesis that is described in the following paragraph seems to be more feasible.

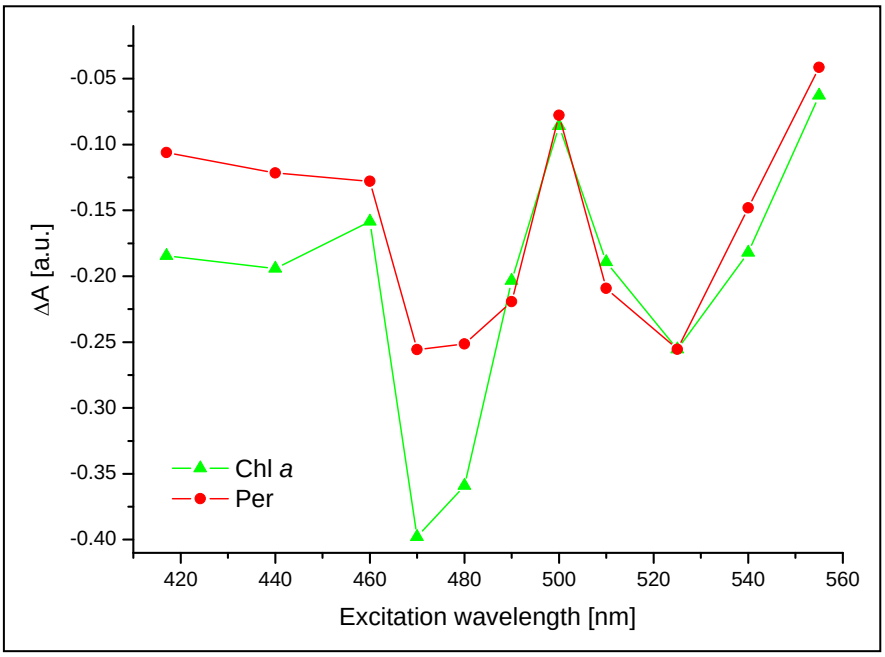

Figure 14: TES of Chl *a* and peridinin; the latter signal is normalized to the one of Chl *a* at 525 nm).

A distinct feature is common to TAS recorded after many excitations[26], i.e. bleaching around 645 nm (see Fig. 11) attributed to Chl *c* (Hiller et al. 1993). Because the Q_y state of Chl *c* is higher than that of Chl *a*, energy transfer to Chl *a* can proceed. Figure 11B better illustrates the situation. For short Δt of 200 fs, the 645-nm bleaching is quite significant, but it disappears at longer delays. The disappearance of the 645-nm bleaching is accompanied by a further increase of the Chl *a* bleaching. More interestingly, Chl *c* feature is present for most of the excitations, for which the other energy transfer channel to Chl *a* (apart from peridinin) is necessary (see Figure 14). Thus the UC seems not to be involved, at least from its S_1 state, in energy transfer to a considerable extent.

To summarize, for excitations below 500 nm the TES of both carotenoids are very similar, but pronounced differences appear for the reddest excitation wavelengths. Carotenoid-Chl energy transfer proceeds mainly from peridinin to Chl *a*, the contribution of UC being rather negligible. The Chl *c*-Chl *a* energy transfer, as proposed by Polívka et al. (2006), was confirmed for the excitation wavelengths falling into the spectral region of Chl *c* absorption. Direct excitation of Chl *a* is the other process contributing to *TA* signal of PDCP.

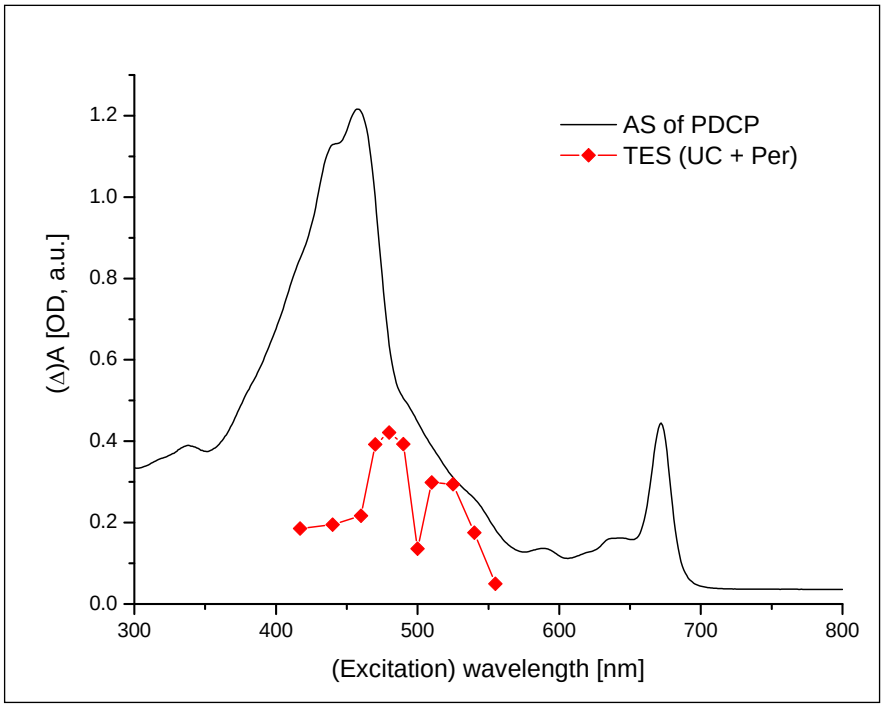

Figure 15: AS of PDCP and TES of added signals from peridinin and UC. The *TA* signals in the TES were magnified to enable the comparison.

Finally, Figure 15 shows the comparison of AS of PDCP and TES of the carotenoids. The TES comprises added *TA* signals of peridinin and UC. It demonstrates that the two shoulders in the AS, peaking around 495 nm and 545 nm, match nicely the peaks in the TES suggesting that the bands in the AS correspond to carotenoids. In particular, to the 495-nm shoulder in the AS contribute both the UC and peridinin while the 540-nm originates almost solely from peridinin (see Fig. 13B). The carotenoid bands in TES are, however, blue-shifted with respect to the bands in the AS. Explanation of this phenomenon is unknown. The fact that peaks in the TES are of different intensity than in the AS can be elucidated

[26] In particular, it is present in TAS after following excitations [nm]: 440, 460, 470, 480, 540 (not that pronounced), and 555.

in such a way that the ratio between extinction coefficients of transitions in the two carotenoids may differ for the steady-state and transient absorption.

3.3 The unidentified carotenoid

Two main hypotheses can be offered regarding the origin of the UC. The first, suggested by Polívka et al. (2006), ascribes the 530-nm signal to diadinoxanthin present in small amounts in PDCP (see Table 2). However, the *TA* signal around 530 nm is comparably strong as that of peridinin for sub-500-nm excitations. Taken this fact into account, it seems unlikely that diadinoxanthin is responsible for the signal in question.

Another fact which should be considered mainly in connection with the first hypothesis is the role of diadinoxanthin as a component of the algal xanthophyll cycle, occurring, among others, in many species of the class Dinophyceae (Frank et al. 1996), member of which is *Amphidinium carterae*. The second component of the cycle is diatoxanthin, having one more conjugated double bond compared to diadinoxanthin. Under high light conditions, diatoxanthin is formed at the expense of diadinoxanthin, which has been correlated with the quenching of Chl fluorescence (Arsalane et al. 1994). Thus any LHC sample should be supplemented with information about light conditions under that the source organisms were cultivated, which was not available for the PDCP studied here. Thus the differences in data measured here and by Polívka et al. (2006) could be caused by different diatoxanthin/diadinoxanthin concentration ratios in the samples (see section 3.2.1 and 3.1).

The second hypothesis concerning the origin of the 530-nm signal is that it emanates from blue-shifted peridinins. This may result from the fact that such peridinins are exposed to different environment, which affects their spectroscopic properties. This idea was also proposed by Papagiannakis et al. (2005) who studied the highly homological FCP using pump-probe spectroscopy. Nevertheless, the comparison should not be oversimplified for two reasons: 1) in FCP, the contained CC is not peridinin, but fucoxanthin; 2) the stoichiometric ratios of pigments are different for the two complexes. Particularly, the diadinoxanthin content in FCP is at least two times lower compared to PDCP, which makes it easier to disregard its influence on TAS. Nevertheless, virtually the same shoulder around 495 nm in the AS was recorded for FCP, which makes the idea of diadinoxanthin to be responsible for the distinct shoulder in either complex improbable. Similarly, the presence of the "blue" peridinin and consequent S_2-S_2 energy transfer between the blue and other peridinins in the PCP complex were proposed by Damjanović et al. (2000).

For above mentioned reasons, the features of the UC (i.e. the band around 495 nm in the AS and the ESA around 530 nm in the TAS) can be assigned to blue-shifted peridinins.

3.4 Global fitting

This procedure was carried out for three main purposes: 1) to correct data for chirp; 2) to obtain fits displayed in graphs in section 3.2.2; 3) to gain information about dynamics of excited states. This section will only deal with the third task.

Excitation wavelength [nm]	1st [ps]	2nd [ps]	3rd [ps]	4th [ps]	5th [ps]
417	<0.1	0.33	1.7	17	200
440		0.30	1.8	17	200
460		0.43	2.6	17	200
470		0.24	2.2	13	200
480		0.38	3.5	22	--
490		0.50	1.1	15	--
500		0.39	3.8	29	--
510		0.33	2.0	14	--
525		0.21	1.0	6	200
540		0.18	1.0	8	200
555		0.46	2.8	10	--
Average (± stdev)	**<0.1**	**0.34 ± 0.10**	**2.1 ± 1.0**	**15 ± 6**	**200**

Table 4: Time constants revealed by global fitting analysis for individual excitations. "1st" means first time constant etc. "Stdev" stands for the standard deviation.

Global fitting analysis revealed that the eleven sets of *TA* data (each set is formed from data obtained after a particular excitation) can be divided into two groups depending on how many time constants were needed to create the EADS (Table 4)[27]. For six excitations (417, 440, 460, 470, 525, and 540 nm) five time constants were used while for the others only four were sufficient. The need for the fifth time constant follows from the fact that significant evolution (mainly in the Chl *a* bleaching region) on tens-of-picoseconds timescale occurs for the six excitations (as an example see Fig. 12C and in it the 440-nm excitation). Furthermore, one non-decaying component (denoted as "inf." in EADS) was necessary in all cases to account for the ~10^{-9} s lifetime of Chl *a* in PDCP (this component is not included in Table 4, but it is depicted in Fig. 16). The time constants averaged for all excitations and dominating processes (according to Polívka et al. 2006) are as follows: sub-0.1 ps (cannot be determined due to limiting time resolution; energy transfer from peridinin S_2 state to Chl *a*), 0.34 ps (energy transfer to Q_y of Chl *a* via hot S_1/ICT state), 2.1 ps (relaxed S_1/ICT-Chl *a* Q_y energy transfer), 15 ps (dynamics connected with the UC), and 200 ps (equilibration/annihilation

[27] The fitting program enables to fix time constants of the components, which is desirable when something is known about the dynamics of a particular system. This is the case of PDCP, so some components were fixed, which explains the striking similarity of some time constants.

processes). This is, however, an oversimplified model because certain distinctions must occur for different excitations. Thus case studies of EADS after excitations at 440 and 480 nm will be presented next.

Fitting of data after 440-nm excitation (Fig. 16A) revealed time constants of sub-0.1, 0.3, 1.8, 17, and 200 ps. The first (black) EADS corresponds to the spectrum of the initially excited state that is a mixture of Chl *a* and S_2 state of carotenoids. It has features typical to carotenoids, i.e. ground state bleaching and the S_2-S_N ESA. The Chl *a* bleaching in this EADS is due to direct Chl *a* excitation. The first EADS is replaced during 100 fs by the second spectrum (red). Here the broad carotenoid region verges to Chl *c* bleaching around 645 nm (Chl *c* may be also directly excited[28]), and Chl *a* bleaching around 674 nm that, except the direct excitation of Chl *a*, might be pronounced also due to energy transfer from S_2 state of peridinin. Another EADS (green) appears with 300-fs time constant. Here the most significant feature is pronounced Chl *a* bleaching (at least partly originating from energy transfer between hot S_1/ICT

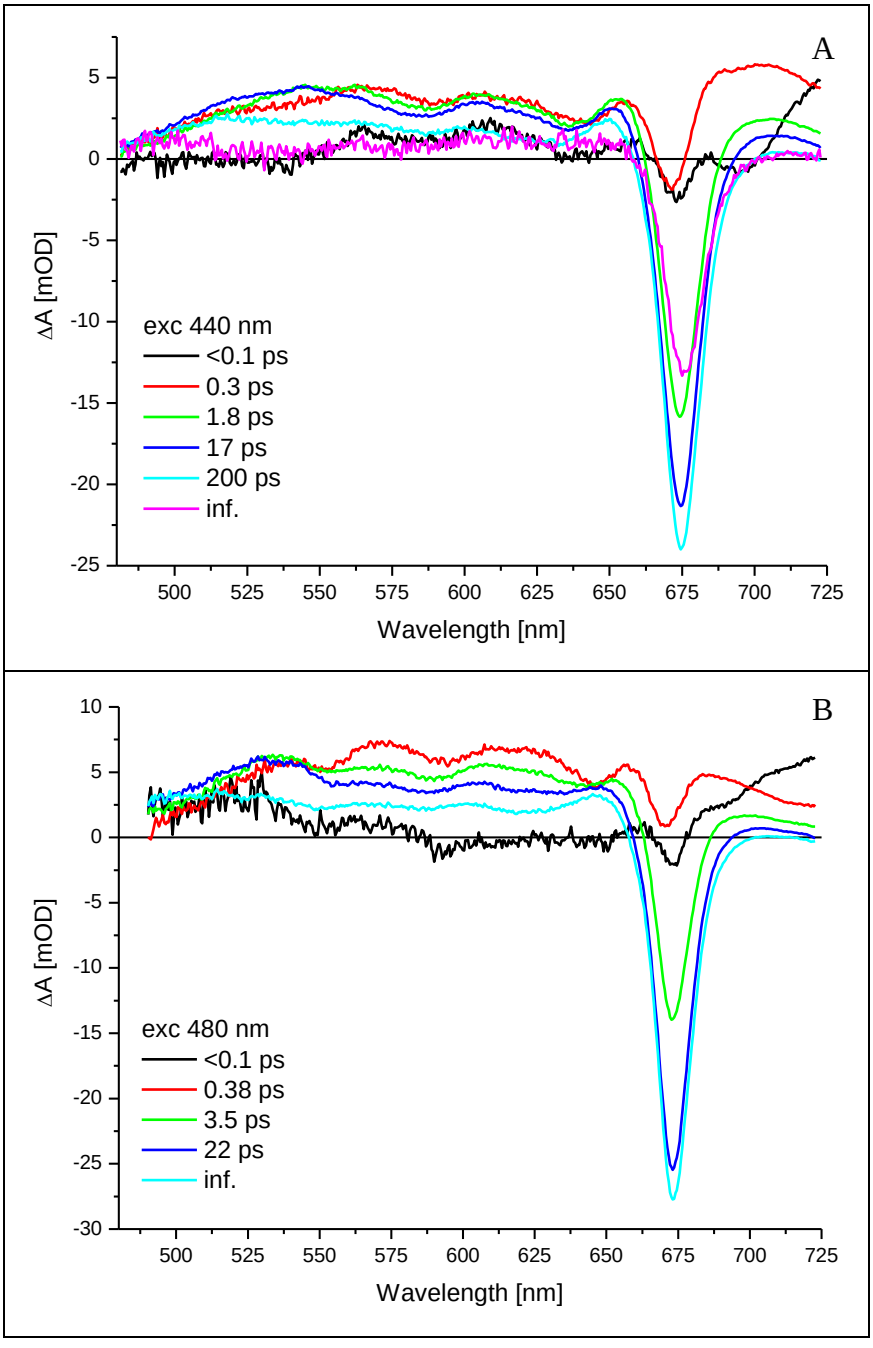

Figure 16: EADS after 440-nm (A) and 480-nm (B) excitation.

[28] Because the pulse duration is ~130 fs, it should not be surprising that bleaching of Chls originating from direct excitation can be deeper in the second EADS than in the first one. Nevertheless, also different processes may participate in deepening of the bleaching, as proposed in the text.

state of peridinin and Chl *a*) and appearing of a shoulder around 540 nm signalling possible involvement of the UC. Next spectrum (blue) emerges within the 1.8-ps step, which is characterized by energy transfer from relaxed S_1/ICT to Chl *a*. Another EADS (cyan) is formed within 17 ps. The ESA in the carotenoid region decreases, which leads to only slight increase of the Chl *a* bleaching. The final non-decaying EADS (magenta) shows the long-lived Chl *a* bleaching signal that is red-shifted, compared to the Chl *a* bleaching in the preceding EADS. Annihilation/equilibration processes between Chls can account for this finding.

EADS after 480-nm excitation are shown in Figure 16B. Four time constants were needed to obtain satisfying fits: sub-0.1, 0.38, 3.5, and 22 ps. The first EADS (black) does not resemble the one after 440-nm excitation in all features, but the early Chl *a* bleaching is obvious here, too. Although the extinction coefficient for Chl *a* at this wavelength is significantly lower, the initial bleaching could still be partly caused by direct excitation of Chl *a*. Moreover, it could arise from the fast energy transfer (from peridinin S_2 state or Chl *c*) that occurs within the time resolution of the measurements. The second EADS (red) is formed on the sub-100-fs time scale and exhibits features of all main pigments: ESA of UC around 535 nm and peridinin probably around both 615 nm and 570 nm; bleaching of Chl *c* around 645 nm and Chl *a* around 673 nm. The evolution towards the third EADS (green) is characterized mainly by the rise of Chl *a* bleaching signal caused by two processes, energy transfer from hot S_1/ICT state of peridinin and from Chl *c* (decrease of signals of both donor pigments is obvious from Figure 16B). The next step occurs within 3.5 ps (blue) and is dominated by the energy transfer from relaxed S_1/ICT state. The non-decaying EADS (cyan) is formed within 22 ps, during which significant decrease of ESA mainly in the region of the UC occurs. Thus the hypothesis of no (the slight rise of Chl *a* bleaching signal can be caused exclusively by energy transfer from peridinin) or only weak energy transfer from the UC is again confirmed.

4. CONCLUSIONS

Main outcomes of this thesis are summarized here:

1) Signals of two main carotenoid species – peridinin and unidentified carotenoid (UC) – present in peridinin diadinoxanthin chlorophyll *a*/*c* protein (PDCP) were extracted in transient excitation spectra (TES), the new method of multi-excitation data interpretation (Fig. 13). This revealed wide-range activity of peridinin in the blue-green region while excitation of the UC was rather restricted to its bluer part.
2) The signal of the UC does most probably not originate from diadinoxanthin. It more likely emanates from blue-shifted peridinins.
3) The involvement of particular carotenoid species in energy transfer differs. While peridinin is the main energy donor in PDCP in the blue-green region (more precisely, from 470 to 555 nm), UC seems not to be involved in energy transfer to a considerable extent. Instead, Chl *c* might be the other important source of excitation energy for Chl *a* apart from its direct excitation.

REFERENCES

Arsalane, W., Rousseau, B., Duval, J.-C. (1994) Influence of the pool size of the xanthophyll cycle on the effects of light stress in a diatom: competition between photoprotection and photoinhibition. *Photochem. Photobiol. 60*, 237–243.

Bassi, R., Caffari, S. (2000) Lhc proteins and the regulation of photosynthetic light harvesting function by xanthophylls. *Photosynth. Res. 64*, 243-256.

Bautista, J.A., Connors, R.E., Raju, B.B., Hiller, R.G., Sharples, F.P., Gosztola, D., Wasielewski, M.R., Frank, H.A. (1999) Excited state properties of peridinin: Observation of a solvent dependence of the lowest excited singlet state lifetime and spectral behavior unique among carotenoids. *J. Phys. Chem. B 103*, 8751-8758.

Bondarev, S.L., Knyukshto, V.N. (1994) Fluorescence from the S_1 (2^1A_g) state of all-trans-β-carotene. *Chemical Physics Letters 225*, 346-350.

Cogdell, R.J. (1985) Carotenoids in photosynthesis. *Pure & Appl. Chem. 57*, 723—728.

Damjanović, A., Ritz, T., Schulten, K. (2000) Excitation transfer in the peridinin-chlorophyll-protein of *Amphidinium carterae*. *Biophys. J. 79*, 1695–1705.

Frank, H.A., Josue, J.S., Bautista, J.A., van der Hoef, I., Jansen, F.J., Lugtenburg, J., Wiederrecht, G., Christensen, R.L. (2002) Spectroscopic and photochemical properties of open-chain carotenoids. *J. Phys. Chem. B 106*, 2083-2092.

Frank, H.A., Bautista, J.A., Josue, J., Pendon, Z., Hiller, R.G., Sharples, F.P., Gosztola, D., Wasielewski, M.R. (2000) Effect of the solvent environment on the spectroscopic properties and dynamics of the lowest excited states of carotenoids. *J. Phys. Chem. B 104*, 4569-4577.

Frank, H.A., Cua, A., Chynwat, V., Young, A., Gosztola, D., Wasielewski, M.R. (1996) The lifetimes and energies of the first excited singlet states of diadinoxanthin and diatoxanthin: the role of these molecules in excess energy dissipation in algae. *Biochim. Biophys. Acta 1277*, 243-252.

Gaier, K., Angerhofer A., Wolf H.C. (1991) The lowest excited electronic singlet states of all-trans β-carotene single crystals. *Chemical Physics Letters 187*, 103-109.

Gilbert, A., Baggott, J. (1991) Essentials of Molecular Photochemistry. CRC Press, London, UK.

Green, B.R., Anderson, J.M., Parson, W.W. (2003) Photosynthetic membranes and their light-harvesting antennas. In Green, B.R. and Parson, W.W. (eds): Light-Harvesting Antennas in Photosynthesis, pp.1-28, Kluwer Academic Publishers, The Netherlands.

Hiller, R.G., Wrench, P.M., Gooley, A.P., Shoebridge, G., Breton, J. (1993) The major intrinsic light-harvesting protein of *Amphidinium:* characterization and relation to other light-harvesting proteins. *Photochemistry and Photobiology 57,* 125-131.

Hiller, R.G., Wrench, P.M., Sharples, F.P. (1995) The light-harvesting chlorophyll *a*-*c*-binding protein of dinoflagellates: a putative polyprotein. *FEBS Letters 363,* 175-178.

Hofmann, E., Wrench, P., Sharples, F.P., Hiller, R.G., Welte, W., Diederichs, K. (1996) Structural basis of light harvesting by carotenoids: Peridinin-chlorophyll-protein from *Amphidinium carterae*. *Science 272*, 1788-1791.

Koka, P., Song, P.-S. (1977) The chromophore topography and binding environment of peridinin chlorophyll *a* protein complexes from marine dinoflagellate algae. *Biochim. Biophys. Acta 495*, 220-231.

Papagiannakis, E., van Stokkum, I.H.M., Fey, H., Büchel, C., van Grondelle, R. (2005) Spectroscopic characterization of the excitation energy transfer in the fucoxanthin-chlorophyll protein of diatoms. *Photosynth. Res. 86*, 241-250.

Polívka, T., Herek, J.L., Zigmantas, D., Åkerlund, H.E., Sundström, V. (1999) Direct observation of the (forbidden) S-1 state in carotenoids. *Proc. of the Nat. Acad. of Sciences of the USA 96*, 4914-4917.

Polívka, T., Sundström, V. (2004) Ultrafast dynamics of carotenoid excited states. From solution to natural and artificial systems. *Chemical Reviews 104*, 2021-2072.

Polívka, T., van Stokkum, I.H.M. Zigmantas, D., van Grondelle, R. Sundström, V., Hiller, R.G. (2006) Energy transfer in the major intrinsic light-harvesting complex from *Amphidinium carterae*. *Biochemistry 45*, 8516-8526.

Sharples, F.P., Wrench, P.M., Ou, K.L., Hiller, R.G. (1996) Two distinct forms of the peridinin-chlorophyll alpha-protein from *Amphidinium carterae*. *Biochim. Biophys. Acta 1276*, 117-123.

Stomp, M., Huisman, J., Stal, L.J., Matthijs, H.C. (2007) Colorful niches of phototrophic microorganisms shaped by vibrations of the water molecule. *ISME Journal 1*, 271–282.

Šetlík, I., Seidlová, F., Šantrůček, J. Textbook to the Plant Physiology Course, Faculty of Science, České Budějovice, electronic publication, http://kfr.prf.jcu.cz.

van Grondelle, R. (1985) Excitation energy transfer, trapping, and annihilation in photosynthetic systems. *Biochim. Biophys. Acta 811*, 147-195.

van Stokkum, I.H.M., Larsen, D.S., van Grondelle, R. (2004) Global and target analysis of time-resolved spectra. *Biochim. Biophys. Acta 1657*, 82-104.

Zigmantas, D., Hiller, R.G., Yartsev, A., Sundström, V., Polívka, T. (2003) Dynamics of excited states of the carotenoid peridinin in polar solvents. Dependence on excitation wavelength, viscosity and temperature. *J. Phys. Chem. B 107*, 5339-5348.

Zigmantas, D., Polívka, T., Hiller, R.G., Yartsev, A., Sundström, V. (2001) Spectroscopic properties of the peridinin lowest singlet excited state. *J. Phys. Chem. A 105*, 10296-10306.

Zimmermann, J., Linden, P.A., Vaswani, H.M., Hiller, R.G., Fleming, G.R. (2002) Two-photon excitation study of peridinin in benzene and in the peridinin chlorophyll a-protein (PCP). *J. Phys. Chem. B 106*, 9418-9423.